Clinical and Translational Report

Cell Metabolism

Osteocalcin Signaling in Myofibers Is Necessary and Sufficient for Optimum Adaptation to Exercise

Graphical Abstract

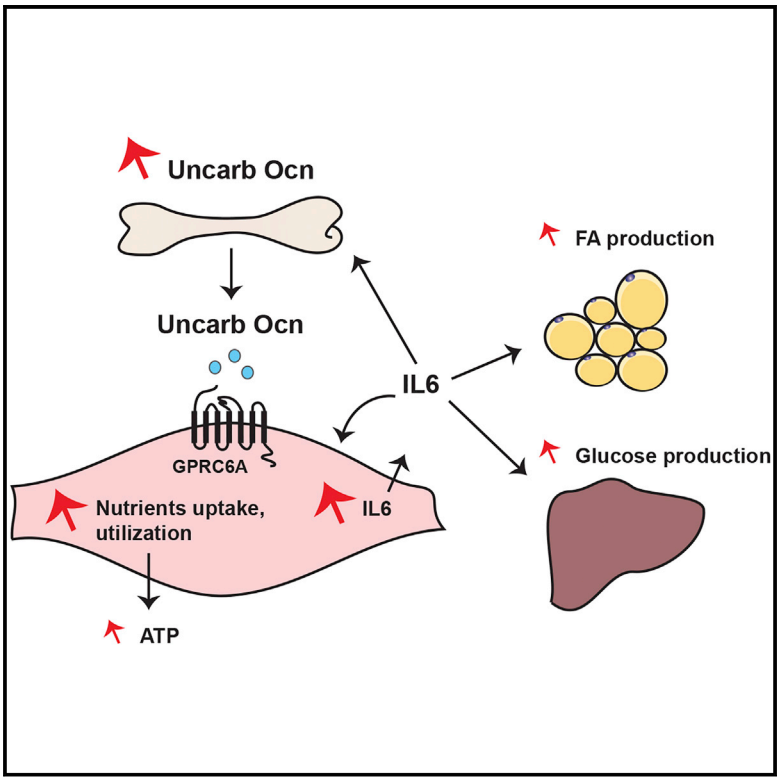

Authors

Paula Mera, Kathrin Laue, Mathieu Ferron, ..., Michelle Puchowicz, Irwin Kurland, Gerard Karsenty

Correspondence

gk2172@cumc.columbia.edu

In Brief

Mera et al. show that the bone-derived hormone osteocalcin is necessary for optimum exercise capacity and that this hormone decreases with aging in mice, monkeys, and humans of both genders. Osteocalcin promotes muscle uptake and utilization of glucose and lipids during exercise and greatly improves the exercise capacity of old mice.

Highlights

- Bone via the hormone osteocalcin improves muscle function during exercise
- Circulating osteocalcin levels decrease in aging mice, monkeys, and humans
- Osteocalcin promotes muscle uptake and utilization of glucose and fatty acids
- Osteocalcin promotes muscle IL-6 secretion during exercise

Mera et al., 2016, Cell Metabolism *23*, 1078–1092
June 14, 2016
http://dx.doi.org/10.1016/j.cmet.2016.05.004

CellPress

Cell Metabolism
Clinical and Translational Report

Osteocalcin Signaling in Myofibers Is Necessary and Sufficient for Optimum Adaptation to Exercise

Paula Mera,[1] Kathrin Laue,[1] Mathieu Ferron,[1,11] Cyril Confavreux,[2] Jianwen Wei,[1] Marta Galán-Díez,[3] Alain Lacampagne,[4] Sarah J. Mitchell,[5] Julie A. Mattison,[5] Yun Chen,[6] Justine Bacchetta,[2] Pawel Szulc,[2] Richard N. Kitsis,[6] Rafael de Cabo,[5] Richard A. Friedman,[7] Christopher Torsitano,[8] Timothy E. McGraw,[8] Michelle Puchowicz,[9] Irwin Kurland,[10] and Gerard Karsenty[1,*]

[1]Department of Genetics and Development, Columbia University Medical Center, New York, NY 10032, USA
[2]INSERM UMR1033-Université de Lyon, Hospices Civils de Lyon, Lyon 69003, France
[3]Department of Physiology and Cellular Biophysics, Columbia University Medical Center, New York, NY 10032, USA
[4]UMR 9214 CNRS, U1046 INSERM, Université de Montpellier, CHRU Montpellier, 34295 Montpellier Cedex 5, France
[5]Translational Gerontology Branch, National Institute on Aging, NIH, Baltimore, MD 21224, USA
[6]Department of Medicine (Cardiology), Department of Cell Biology, and Wilf Family Cardiovascular Research Institute, Albert Einstein College of Medicine, Bronx, NY 10461, USA
[7]Department of Biomedical Informatics, Columbia University Medical Center, New York, NY 10032, USA
[8]Department of Biochemistry, Weill Medical College of Cornell University, New York, NY 10065, USA
[9]Department of Nutrition, School of Medicine, Case Western Reserve University, Cleveland, OH 44106, USA
[10]Department of Medicine, Albert Einstein College of Medicine, Bronx, NY 10461, USA
[11]Present address: Integrative and Molecular Physiology Research Unit, Institut de Recherche Clinique de Montréal, Montréal, QC H2W 1R7, Canada
*Correspondence: gk2172@cumc.columbia.edu
http://dx.doi.org/10.1016/j.cmet.2016.05.004

SUMMARY

Circulating levels of undercarboxylated and bioactive osteocalcin double during aerobic exercise at the time levels of insulin decrease. In contrast, circulating levels of osteocalcin plummet early during adulthood in mice, monkeys, and humans of both genders. Exploring these observations revealed that osteocalcin signaling in myofibers is necessary for adaptation to exercise by favoring uptake and catabolism of glucose and fatty acids, the main nutrients of myofibers. Osteocalcin signaling in myofibers also accounts for most of the exercise-induced release of interleukin-6, a myokine that promotes adaptation to exercise in part by driving the generation of bioactive osteocalcin. We further show that exogenous osteocalcin is sufficient to enhance the exercise capacity of young mice and to restore to 15-month-old mice the exercise capacity of 3-month-old mice. This study uncovers a bone-to-muscle feedforward endocrine axis that favors adaptation to exercise and can reverse the age-induced decline in exercise capacity.

INTRODUCTION

The ability to perform exercise is an evolutionary conserved function that has been essential for the survival of most vertebrates and nowadays has significant health benefits (Neufer et al., 2015; Zierath and Wallberg-Henriksson, 2015). During exercise, muscle function needs to significantly increase; this requires that the uptake and catabolism of the two main nutrients of myofibers, glucose and fatty acids (FAs), markedly rise (Hawley et al., 2014). As an anabolic hormone, insulin promotes glucose uptake in myofibers and stores it in the form of glycogen post-prandially (Saltiel and Pessin, 2002). However, insulin does not promote glucose catabolism, and its circulating levels decline during exercise (Coderre et al., 1995; Lund et al., 1995). This suggests that the rise in nutrient uptake and in their catabolism in muscle that occurs during exercise may be favored by other secreted molecules, myokines (Catoire and Kersten, 2015) or hormones, the circulating levels of which would increase during exercise. Conceivably, myokines and hormones may cooperate to favor adaptation to exercise.

The ability of bone to sense mechanical forces, the physical proximity of the two tissues, and the fact that exercise capacity and bone mass decline at the same time have long suggested that a crosstalk between bone and muscle may exist (Novotny et al., 2015). The recent identification of bone-derived hormones and of their receptors allows us to test if bone regulates muscle function at rest or during exercise and to elucidate the molecular bases of this function. Another reason to ask this question arises from a feature of the bone-derived hormone osteocalcin: this hormone favors physiological functions that, like memory and male fertility, greatly decline with age (Oury et al., 2011, 2013). This observation raises the possibility that osteocalcin may regulate other physiological processes severely affected by aging, such as muscle function during exercise (Partridge and Gems, 2002).

In testing this hypothesis, we observed that the circulating levels of osteocalcin double during endurance exercise in young adult wild-type (WT) mice, decrease sharply before or around mid-life in all species tested, and do not increase during exercise in older mice to the same extent as in young mice. Exploring these observations revealed that osteocalcin signaling in

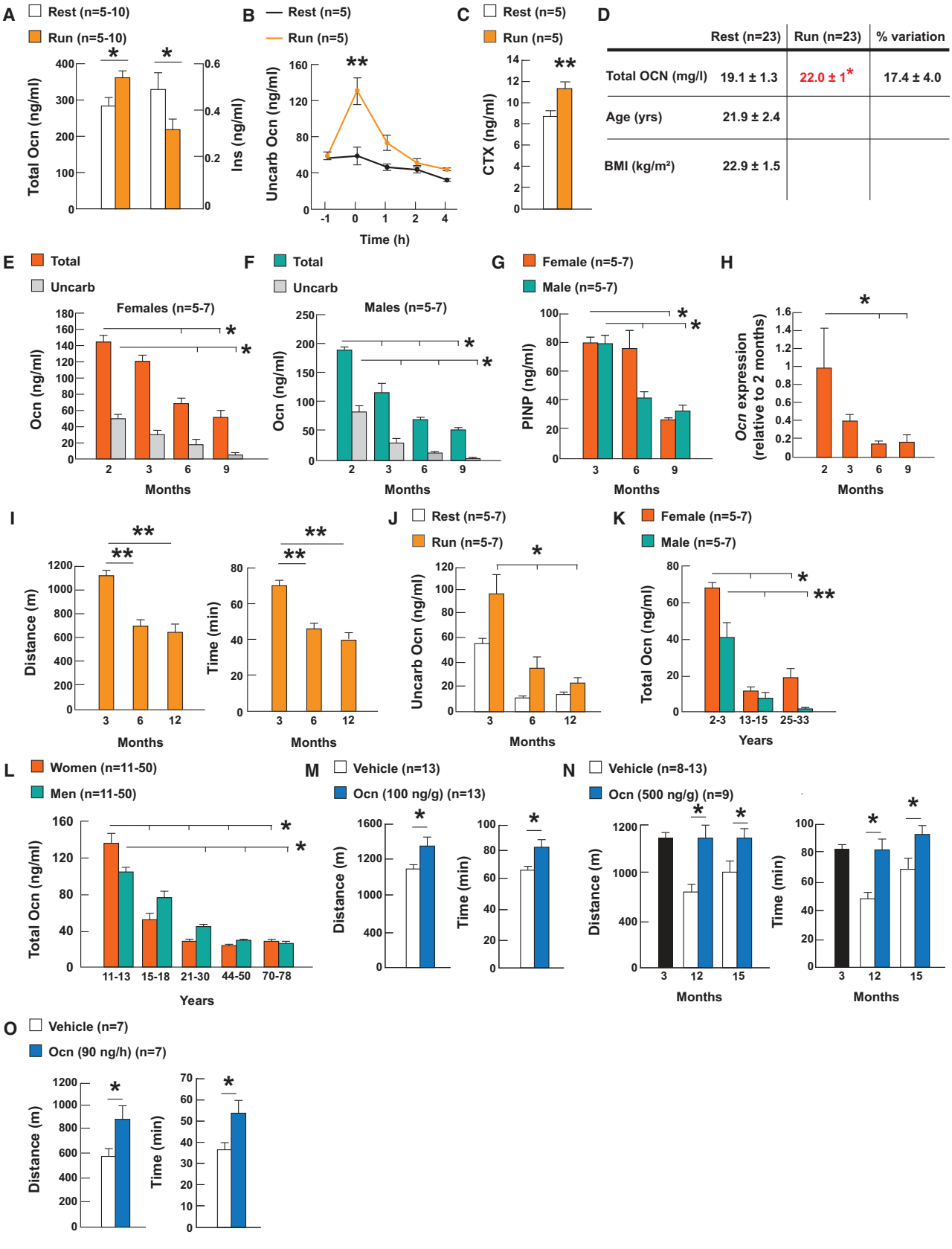

(legend on next page)

myofibers favors adaptation to exercise in part because it promotes the uptake and catabolism of glucose and FAs. These observations explain why exogenous osteocalcin restores the exercise capacity of 15-month-old mice to that of 3-month-old mice. In addition to its regulation of nutrient uptake and catabolism, osteocalcin signaling in myofibers is also responsible for most of the exercise-induced increase in the circulating levels of interleukin-6 (IL-6), a myokine that promotes adaptation to exercise in part by increasing the production of bioactive osteocalcin. Hence, a feedforward regulation linking together the endocrine functions of bone and muscle appears to be necessary and sufficient to favor adaptation to exercise.

RESULTS

Regulation of Osteocalcin by Exercise and Age

The growing number of functions ascribed to osteocalcin (Karsenty and Olson, 2016) raises the question of whether the circulating levels of this hormone change in various physiological situations. This analysis revealed that a single bout of endurance aerobic-based exercise (40 min run on a treadmill at 30 cm/s, 80% VO_2 max, thereafter referred to as exercise) increased circulating osteocalcin levels of total, undercarboxylated, and bioactive 2-fold in 3-month-old WT mice, while at same time the circulating levels of insulin decreased. This increase in the circulating levels of bioactive osteocalcin was due in part to an increase in bone resorption, the arm of bone remodeling that is responsible for osteocalcin decarboxylation and activation (Ferron et al., 2010) (Figures 1A–1C). Circulating osteocalcin levels also significantly increased in young women after a 45 min-long exercise (Figure 1D).

In contrast, circulating osteocalcin levels greatly decreased in all species tested in another physiological situation, aging. Indeed, whether we measure total or undercarboxylated circulating osteocalcin, these levels decreased by 70% in male and female mice between 2 and 9 months of age. This was due to a decline in *Osteocalcin* expression and in bone formation as measured by serum PINP levels (Figures 1E–1H). This decrease in circulating osteocalcin levels occurs at the time the ability of mice to perform exercise declines, and circulating osteocalcin levels do not increase to the same extent in 6- or 12-month-old mice as in 3-month-old mice during exercise (Figures 1I and 1J). The same decrease in circulating osteocalcin levels was seen in male and female rhesus monkeys between young (2–3 years) and middle age (13–15 years) (Figure 1K). In humans, circulating osteocalcin levels reach their lowest point before 30 years old in women and 50 years old in men (Figure 1L).

The increase of circulating osteocalcin levels during exercise, and their decrease with age when exercise capacity declines, led us to test whether exogenous osteocalcin could increase the exercise capacity of older WT mice. In a proof-of-principle experiment, we first asked whether one intraperitoneal (i.p.) injection of uncarboxylated mouse osteocalcin (osteocalcin) (100 ng/g of body weight) immediately before exercise would improve the exercise capacity of 3-month-old WT mice. This injection raised circulating osteocalcin levels without affecting those of insulin (Figures S1A and S1B, available online) and increased the time and distance these mice run on the treadmill at a constant speed (30 cm/s) before exhaustion by over 20% (Figure 1M). In view of these results, 12- and 15-month-old WT mice that have low circulating osteocalcin levels were injected with osteocalcin (500 ng/g of body weight) prior to exercise. This injection increased circulating osteocalcin levels more than 4-fold and conferred to these older mice the ability to run the same time and distance as 3-month-old untreated WT mice (Figures S1C and 1N). Chronic delivery of osteocalcin through mini-pumps (90 ng/hour) for 28 days also increased circulating osteocalcin levels without affecting those of insulin (Figures S1D and S1E), as well as the time and distance 10-month-old WT mice run on a treadmill before exhaustion (Figure 1O). Thus, exogenous osteocalcin is sufficient to reverse the age-induced decrease in exercise capacity in mice.

Osteocalcin Signaling in Myofibers Is Necessary for Adaptation to Exercise

The observations presented above raised the question of whether osteocalcin is necessary for adaptation to exercise. Given the influence of testosterone on physical activity and the low circulating testosterone levels in male *Osteocalcin* (*Ocn*)$^{-/-}$ mice, this question was addressed in female mice.

When forced to run on a treadmill at a constant speed until exhaustion, 3-, 6-, and 9-month-old *Ocn*$^{-/-}$ mice run 20% to 30% less time and distance than WT littermates (Figures 2A and S2A). Since exercise capacity may vary even in genetically identical animals, experiments testing exercise capacity were conducted in several cohorts of control and mutant mice (n = 8–13 per group). This reflected the absence of a signaling event from bone to muscle since the same decline in exercise capacity

Figure 1. Regulation of Circulating Osteocalcin Levels by Exercise and Age

(A) Serum total osteocalcin (Ocn) and insulin (Ins) levels in 3-month-old mice at rest or after exercise.
(B) Serum undercarboxylated Ocn (uncarb Ocn) levels in 3-month-old mice at rest (−1) and 0, 1, 2, and 4 hr after exercise.
(C) Serum CTX levels in 3-month-old mice at rest and after exercise.
(D) Serum OCN levels in women at rest and after exercise.
(E and F) Serum total and uncarb Ocn levels in female (E) and male (F) mice of various ages.
(G) Serum PINP in mice of various ages.
(H) *Osteocalcin* (*Ocn*) expression in femur in mice of various ages.
(I) Performance during an endurance test (running on a treadmill at 30 cm/s until exhausted) of 3-, 6-, and 12-month-old female WT mice.
(J) Serum uncarb Ocn levels in 3-, 6-, and 12-month-old female mice at rest and after exercise.
(K) Serum total Ocn levels in 2- to 33-year-old female and male rhesus macaque monkeys.
(L) Serum total OCN levels in women and men 11 to 78 years old.
(M–O) (M) Performance during an endurance test (running on a treadmill at 30 cm/s until exhausted) of 3-month-old and (N) 12- and 15-month-old WT mice treated with Ocn, and (O) 10-month-old WT mice receiving Ocn for 28 days.
(Exercise refers to 40 min running at 30 cm/s on a treadmill.) All data are presented as mean ± SEM.

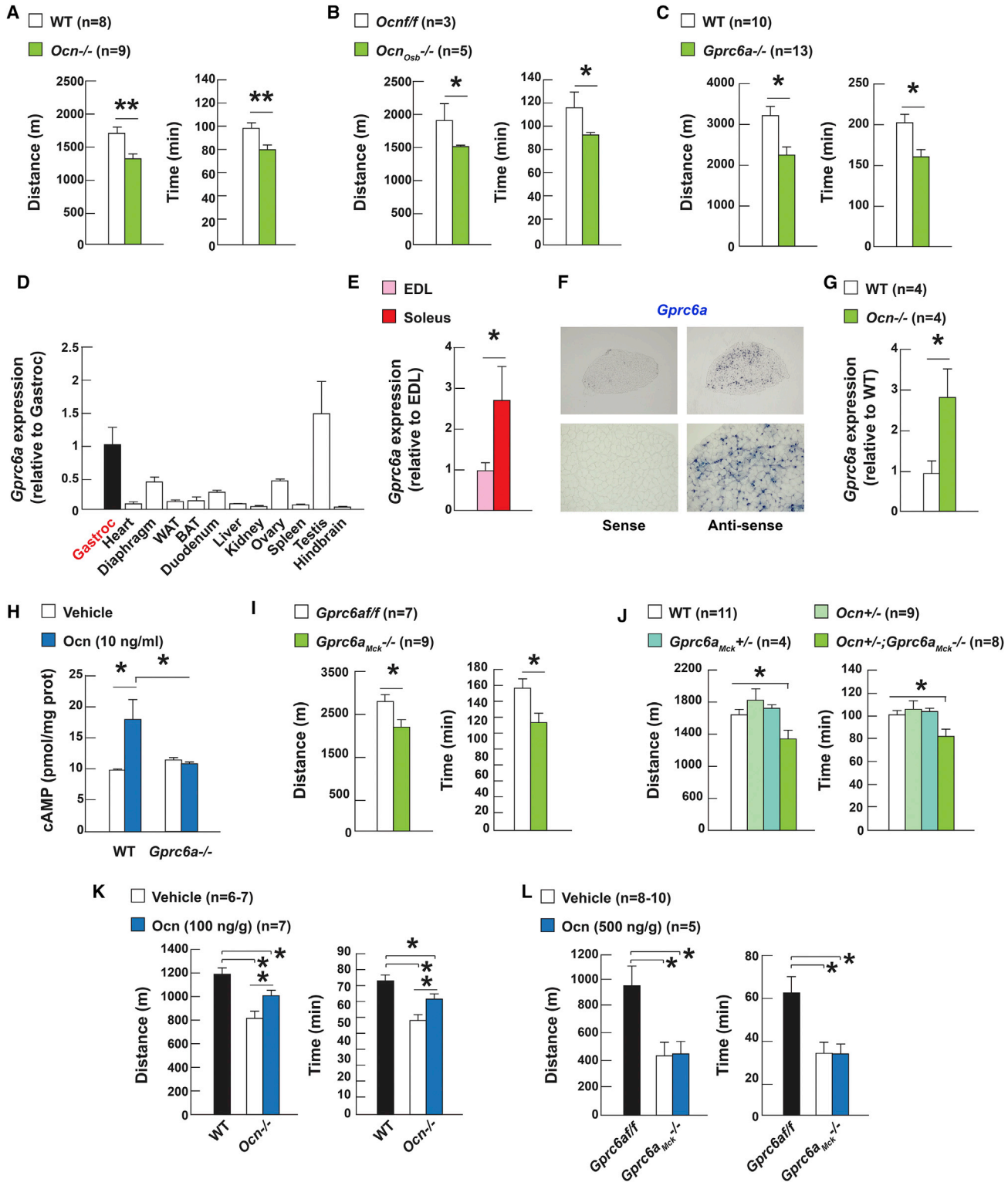

Figure 2. Osteocalcin Signaling in Myofibers Is Necessary for Adaptation to Exercise

(A–C) (A) Performance during an endurance test (running on a treadmill at 30 cm/s until exhausted) of 3-month-old *Ocn*$^{-/-}$ and WT mice, (B) *Ocn*$^{f/f}$ and *Ocn*$_{Osb}$$^{-/-}$ mice, and (C) *Gprc6a*$^{-/-}$ and WT mice.

(D and E) (D) *Gprc6a* expression in various tissues and (E) in EDL and soleus muscles.

(F) In situ hybridization analysis of *Gprc6a* expression in soleus muscle.

(G) *Gprc6a* expression in WT and *Ocn*$^{-/-}$ gastrocnemius muscles.

(legend continued on next page)

was observed in mice lacking *Osteocalcin* only in osteoblasts and post-natally (Figure 2B). Accordingly, this decline in exercise capacity was not observed in 2-month-old $Ocn^{-/-}$ mice, indicating that the osteocalcin regulation of exercise capacity is not of developmental origin (Figure S2B). The same decrease in exercise capacity was observed in several cohorts of 3-month-old mice lacking Gprc6a, the osteocalcin receptor (Oury et al., 2011) (Figure 2C).

$Ocn^{-/-}$ and $Gprc6a^{-/-}$ mice display metabolic and/or behavioral abnormalities that make the interpretation of any phenotype linked to exercise difficult. To exclude these confounding factors and determine if osteocalcin promotes adaptation to exercise by signaling in skeletal muscle, we studied *Gprc6a* expression in this tissue. A qPCR survey showed that *Gprc6a* was more highly expressed in skeletal muscles than in most tissues, and more so in oxidative muscles (soleus) that are needed for a prolonged effort than in glycolytic muscles (EDL), and an in situ hybridization analysis demonstrated that *Gprc6a* is expressed in myofibers (Figures 2D–2F). Moreover, *Gprc6a* expression was 3-fold higher in $Ocn^{-/-}$ than in WT muscle, and osteocalcin did not increase cAMP production in $Gprc6a^{-/-}$ myotubes as it did in WT ones (Figures 2G and 2H). In view of these data suggesting that Gprc6a mediates osteocalcin signal in myofibers, we deleted *Gprc6a* from myofibers by crossing mice harboring a floxed allele of *Grpc6a* with *Mck-Cre* deleter mice (Brüning et al., 1998). *Gprc6a* expression was decreased over 50% in skeletal muscles in $Gprc6a_{Mck}^{-/-}$ mice (Figure S2C). Body composition, glucose tolerance, and insulin sensitivity were similar in $Gprc6a_{Mck}^{-/-}$ and control mice (Figures S2D–S2F).

Starting at 3 months of age, all cohorts of $Gprc6a_{Mck}^{-/-}$ mice experienced a decrease in exercise capacity that was of equal severity as the one noted in $Ocn^{-/-}$ mice (Figure 2I). This could not be explained by a disruption of the intrinsic properties of muscle since excitation-contraction coupling and resistance to fatigue were not lower in $Gprc6a_{Mck}^{-/-}$ than in control muscles. Fiber type composition and size were also the same in muscles of $Gprc6a_{Mck}^{-/-}$ and control mice (Figures S2G–S2I). That a similar decrease in exercise capacity was seen in compound mutant mice lacking one allele of *Osteocalcin* and one allele of *Gprc6a* in myofibers ($Ocn^{+/-}$;$Gprc6a_{Mck}^{+/-}$) provides a genetic support to the notion that osteocalcin is the ligand of Gprc6a in myofibers that is responsible for *Gprc6a* regulation of adaptation to exercise (Figure 2J). Moreover, a single injection of osteocalcin increased the exercise capacity of $Ocn^{-/-}$ mice, but did not do so in $Gprc6a_{Mck}^{-/-}$ mice (Figures 2K and 2L). At the same time, multiple evidences suggest that the ability of osteocalcin to favor adaptation to exercise is not secondary to its signaling in the heart: *Gprc6a* expression is 20-fold lower in the heart than in skeletal muscle (Figure 2D), heart function is normal in $Ocn^{-/-}$ and $Gprc6a_{Mck}^{-/-}$ mice, and deleting *Gprc6a* only in cardiomyocytes does not affect exercise capacity in mice (Figures S2J–S2L).

Osteocalcin Signaling in Myofibers Promotes Uptake and Catabolism of Glucose during Exercise

To determine how osteocalcin signaling in myofibers favors adaptation to exercise, we used indirect calorimetry to measure nutrient utilization and aerobic capacity in $Gprc6a_{Mck}^{-/-}$ and control mice running on a treadmill at an increasing speed (initial speed 5 cm/s and increasing by 3 cm/s every minute until exhaustion). In the conditions of this assay, the maximal oxygen consumption was significantly decreased in $Gprc6a_{Mck}^{-/-}$ mice, whereas their respiratory exchange ratio (RER) was not affected (Figures 3A–3C). These results suggesting that osteocalcin signaling in myofibers promotes aerobic capacity during exercise prompted us to test if osteocalcin signaling in myofibers affects mitochondrial number/respiration and/or uptake and utilization of nutrients.

The number of mitochondria in muscles was the same in 3-month-old $Ocn^{-/-}$ mice that already have a poor exercise capacity, and WT littermates. Expression of a transcriptional determinant of mitochondrial biogenesis and muscle adaptation to exercise, *Pgc1α* (Da Cruz et al., 2012; Handschin and Spiegelman, 2008), and of its target genes was similar in muscles of $Ocn^{-/-}$, $Gprc6a_{Mck}^{-/-}$, and control mice after exercise. The activities of the mitochondrial proteins COX and SDH were the same in $Gprc6a_{Mck}^{-/-}$ and control muscles after exercise, and there was no detectable difference in mitochondrial respiration between WT and $Gprc6a^{-/-}$ myofibers that were cultured in the presence of glucose, pyruvate, and amino acids (Figures S3A–S3G). Given their negative nature, these results need to be interpreted cautiously, yet they indicate that the ability of osteocalcin signaling in myofibers to favor adaptation to exercise is not secondary to a measurable effect on mitochondrial number or function. Hence, we turned our attention to nutrient uptake and catabolism during exercise.

The main nutrient used by muscle to generate energy at the onset of exercise is glucose that is stored in myofibers in the form of glycogen (Lehninger et al., 2000). Glycogen breakdown measured by the difference between glycogen content at rest and after exercise was lower in $Gprc6a_{Mck}^{-/-}$ and $Ocn^{-/-}$ muscle than in control ones (Figures 3D and S3H). In contrast, liver glycogen breakdown was the same in $Gprc6a_{Mck}^{-/-}$ and control mice (Figure S3I). Furthermore, osteocalcin enhanced glucose uptake, as determined by the uptake of ^{3}H-2-deoxyglucose (^{3}H-2DG), in WT, but not in $Gprc6a^{-/-}$, myotubes. The same was true in WT isolated soleus treated with osteocalcin (Figures 3E, 3F, and S3J). In vivo, the uptake of ^{3}H-2DG was significantly increased in oxidative muscles in WT mice receiving osteocalcin prior to exercise but was decreased in those of $Gprc6a_{Mck}^{-/-}$ mice after exercise (Figures 3G and 3H). Lastly, osteocalcin favored glycolysis, defined by the extracellular acidification of the media (ECAR), in WT, but not in $Gprc6a^{-/-}$, myofibers (Figure 3I). Importantly, none of the

(H) cAMP accumulation in WT and $Gprc6a^{-/-}$ myotubes treated with vehicle or osteocalcin (Ocn).

(I and J) (I) Performance during an endurance test (running on a treadmill at 30 cm/s until exhausted) of 3-month-old $Gprc6a^{f/f}$ and $Gprc6a_{Mck}^{-/-}$ mice and (J) $Ocn^{+/-}$;$Gprc6a_{Mck}^{+/-}$ and control mice.

(K and L) (K) Performance during an endurance test (running on a treadmill at 30 cm/s until exhausted) of 6-month-old $Ocn^{-/-}$ or (L) 12-month-old $Gprc6a_{Mck}^{-/-}$ mice treated with Ocn.

All data are presented as mean ± SEM.

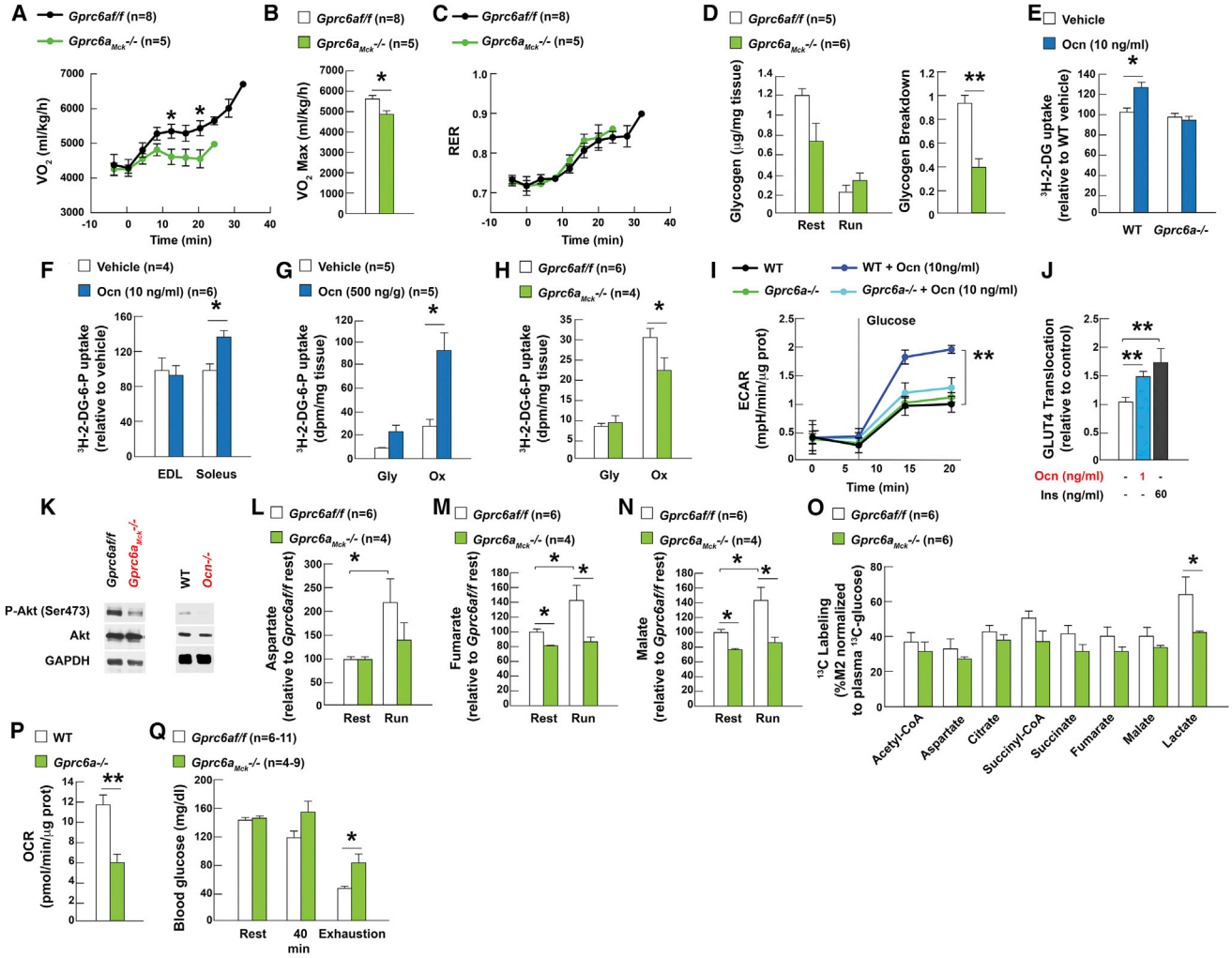

Figure 3. Osteocalcin Signaling in Myofibers Promotes Uptake and Utilization of Glucose during Exercise

(A–C) (A) VO_2, (B) VO_2 max, and (C) RER in 3-month-old *Gprc6a*$^{f/f}$ and *Gprc6a*$_{Mck}$$^{-/-}$ mice running on a treadmill at increasing speed until exhausted.

(D) Glycogen content and breakdown in 3-month-old *Gprc6a*$^{f/f}$ and *Gprc6a*$_{Mck}$$^{-/-}$ tibialis muscles at rest and after exercise.

(E and F) (E) Uptake of ^{3}H-2-deoxyglucose (^{3}H-2-DG) in WT and *Gprc6a*$^{-/-}$ myotubes and (F) WT EDL and soleus muscles treated with vehicle or osteocalcin (Ocn).

(G and H) (G) Uptake of ^{3}H-2-DG in glycolytic (Gly, white quadriceps) and oxidative (Ox, red quadriceps) muscles after exercise in 3-month-old *Gprc6a*$^{f/f}$ and *Gprc6a*$_{Mck}$$^{-/-}$ mice and (H) 15-month-old WT mice treated with Ocn.

(I) Glycolysis, determined by the extracellular acidification of the media (ECAR), in WT and *Gprc6a*$^{-/-}$ myofibers treated with vehicle or Ocn.

(J) GLUT4 translocation in C2C12 myoblasts treated with Ocn, determined by optic microscopy.

(K) Western blot analyses of Akt phosphorylation (Ser473) in tibialis muscles of 3-month-old *Gprc6a*$^{f/f}$, *Gprc6a*$_{Mck}$$^{-/-}$, WT, and *Ocn*$^{-/-}$ mice after exercise.

(L–N) (L) Aspartate and (M and N) TCA cycle metabolite accumulation in quadriceps of 3-month-old *Gprc6a*$^{f/f}$ and *Gprc6a*$_{Mck}$$^{-/-}$ mice at rest and after exercise.

(O) ^{13}C-labeled TCA metabolites and lactate in quadriceps muscles of 3-month-old *Gprc6a*$^{f/f}$ and *Gprc6a*$_{Mck}$$^{-/-}$ mice receiving a bolus of ^{13}C-glucose prior to exercise.

(P) Oxygen consumption rate (OCR) in myofibers cultured in Krebs-Ringer HEPES buffer with 25 mM glucose.

(Q) Blood glucose levels in 3-month-old *Gprc6a*$^{f/f}$ and *Gprc6a*$_{Mck}$$^{-/-}$ mice at rest and after running on a treadmill for 40 min or until exhaustion.

(Exercise refers to 40 min running at 30 cm/s on a treadmill.) All data are presented as mean ± SEM.

other proposed ligands of Gprc6a favored glucose uptake or glycolysis in WT myotubes and myofibers (Figures S3K and S3L).

To promote glucose uptake in muscle osteocalcin does not affect the expression of *Glut1* and *Glut4* (Figure S3M), but rather favors the translocation of GLUT4 to the plasma membrane of C2C12 myoblasts that express *Gprc6a-myc* and HA-*Glut4-Gfp* (Figure 3J). Signaling through GPCRs can promote Akt phosphorylation, an event that is observed in muscles after exercise and that allows the translocation of GLUT4 to the plasma membrane (Deshmukh et al., 2006; Lopez-Ilasaca et al., 1997). We found that Akt phosphorylation was decreased in muscles of *Gprc6*$_{Mck}$$^{-/-}$ and *Ocn*$^{-/-}$ compared to those of control mice after exercise; conversely, acute or chronic administration of osteocalcin induced Akt phosphorylation in WT myotubes and muscle (Figures 3K and S3N–S3P).

To assess the influence of osteocalcin signaling in myofibers on the activity of the TCA cycle, we performed a metabolomics study. This analysis showed that the accumulation of aspartate, a reliable indicator of the cellular levels of the TCA cycle intermediate oxaloacetate, and of fumarate and malate, the two TCA cycle intermediates that increase the most during exercise (Gibala et al., 1998; Sahlin et al., 1990), did not rise to the same extent in muscles of *Gprc6a*$_{Mck}^{-/-}$ as in those of control mice after exercise (Figures 3L–3N). Moreover, the contribution of ^{13}C-glucose to the labeling of each TCA cycle intermediate measured and of lactate was decreased in muscle of *Gprc6*$_{Mck}^{-/-}$ mice injected with ^{13}C-glucose prior to exercise (Figure 3O). This latter result suggests that the lower content of TCA cycle intermediates in *Gprc6a*$_{Mck}^{-/-}$ muscles after exercise reflects in part a decrease in the entry of carbon originating from glucose into the TCA cycle. This decreased uptake and catabolism of glucose in muscle of *Gprc6*$_{Mck}^{-/-}$ mice explains why the oxygen consumption rate (OCR) was 2-fold lower in *Gprc6a*$^{-/-}$ than in WT myofibers when the only nutrient of these myofibers was glucose (Figure 3P). The ability of osteocalcin signaling in myofibers to favor glucose uptake also provides an explanation for the increase in blood glucose levels observed in *Gprc6a*$_{Mck}^{-/-}$ mice running until exhaustion (Figure 3Q).

Osteocalcin Signaling in Myofibers Favors FA Utilization during Exercise

Since FA uptake and oxidation in muscle progressively increase during exercise (Hawley et al., 2014; Koves et al., 2005), we tested if osteocalcin signaling in myofibers also affects these processes during exercise.

We first measured muscle and plasma levels of acylcarnitines, a reliable indicator of FA utilization in cells (Overmyer et al., 2015). We found that the accumulation of long- and medium-chain acylcarnitines seen in muscles of control mice after exercise did not occur nearly to the same extent in muscles of *Gprc6a*$_{Mck}^{-/-}$ mice (Figure 4A). There was instead a significant rise in acylcarnitine accumulation in the plasma of *Gprc6a*$_{Mck}^{-/-}$ mice (Figure 4B). Moreover, the levels of free L-carnitine that significantly declined in muscles of control mice after exercise did not do so to the same extent in those of *Gprc6a*$_{Mck}^{-/-}$ mice (Figure S4A). These results, which suggest that osteocalcin signaling in myofibers is needed for efficient FA catabolism during exercise, explain in part why osteocalcin did not increase ^{14}C-oleate oxidation in *Gprc6a*$^{-/-}$ myotubes as it did in WT ones, and why the OCR of *Gprc6a*$^{-/-}$ myofibers was significantly lower than that of WT ones when oleate was the only substrate of these myofibers (Figures 4C, 4D, and S4B). Plasma non-esterified fatty acid (NEFA) levels were significantly higher in *Gprc6a*$_{Mck}^{-/-}$ than in control mice after exercise, while glycerol levels were unchanged. These results are consistent with the notion that FA uptake and catabolism in muscle are decreased in mice lacking osteocalcin signaling in myofibers (Figures 4E and S4C).

How does osteocalcin favor FA catabolism in myofibers? Once phosphorylated at Thr172, the cellular energy sensor AMPK promotes FA utilization in muscle by increasing the activity of CPT1B, a transporter of long-chain FAs into the mitochondria (O'Neill et al., 2014). AMPK phosphorylation at Thr172 was reduced in muscles of *Gprc6a*$_{Mck}^{-/-}$ compared to those of control mice after exercise, and conversely, exogenous osteocalcin increased AMPK phosphorylation in muscles of WT mice during exercise (Figures 4F and 4G). Likewise, phosphorylation of ACC (Ser79) was decreased and the accumulation of malonyl-CoA was increased in *Gprc6a*$_{Mck}^{-/-}$ muscles after exercise (Figures S4D and S4E). Osteocalcin promotes FA oxidation in muscle in an AMPK-dependent manner, since it induces FA oxidation in WT, but not *Ampkα2*$^{-/-}$, myotubes (Figure 4H). In contrast, osteocalcin favored glucose uptake in an AMPK-independent manner (Figure 4I). Hormone sensitive lipase (HSL) favors hydrolysis of intracellular triglycerides into free FAs in muscle when phosphorylated at Ser563 (Watt and Spriet, 2010). HSL phosphorylation was reduced in muscles of *Gprc6a*$_{Mck}^{-/-}$ and *Ocn*$^{-/-}$ compared to those of control mice, whereas *Hsl* expression was unchanged. Conversely, HSL phosphorylation was increased in muscles of WT mice receiving osteocalcin prior to exercise (Figures 4J, 4K, and S4F).

Furthermore, the expression of *Cd36* and *Fatp1*, which facilitate the uptake of long-chain FAs into cells, and of *Cpt1b*, which promotes their transport across the mitochondrial membrane (Stahl et al., 2001), was decreased in *Gprc6a*$^{-/-}$ myotubes, while osteocalcin increased the expression of *Fatp1*, *Cpt1b*, and, to a lesser extent, *Cd36* in WT myotubes (Figures S5A and S5B). This explains why the expression of *Fatp1*, *Cpt1b*, and *Cd36* did not increase in muscles of *Ocn*$^{-/-}$, *Gprc6a*$_{Mck}^{-/-}$, and *Ocn*$^{+/-}$; *Gprc6a*$_{Mck}^{+/-}$ as they did in those of control mice after exercise and why *Fatp1* expression increased in muscles of WT mice receiving osteocalcin prior to exercise (Figures 5A–5C).

Two observations identify CREB as one mediator of osteocalcin signaling in myofibers. First, CREB phosphorylation was weaker in muscles of *Gprc6a*$_{Mck}^{-/-}$ than in those of control mice after exercise, and stronger in myotubes of WT mice treated with osteocalcin. Second, the exercise capacity of *Gprc6a*$_{Mck}^{+/-}$;*Creb*$_{Mck}^{+/-}$ mice is as decreased as that of *Gprc6a*$_{Mck}^{-/-}$ mice (Figures 5D–5F). Accordingly, CREB mediates osteocalcin regulation of glucose uptake in myotubes and glycolysis in myofibers (Figures 5G and 5H). However, the fact that osteocalcin induces FA oxidation equally well in control and *Creb*$^{-/-}$ myotubes indicates that osteocalcin uses other transcriptional mediators to favor FA oxidation (Figure 5I).

Taken together, these results indicate that osteocalcin signaling in myofibers favors uptake and catabolism of both glucose and FAs in a balanced manner during exercise. These findings imply that osteocalcin signaling should be necessary to generate the ATP required for optimum muscle performance during exercise. In agreement with this hypothesis, ATP levels were significantly lower in muscles of *Gprc6a*$_{Mck}^{-/-}$ mice than in those of control ones after exercise (Figure 5J). This low ATP content, along with the decreased phosphorylation of AMPK, suggests that osteocalcin signaling in myofibers regulates AMPK phosphorylation in part in an AMP-independent manner (Jensen et al., 2007).

Osteocalcin Is Necessary for the Increase in *Interleukin-6* Expression in Muscle Occurring during Exercise

To determine if osteocalcin signaling in myofibers favors adaptation to exercise through additional mechanisms, we performed a transcriptomic analysis in muscles of control and *Gprc6a*$_{Mck}^{-/-}$ mice after exercise.

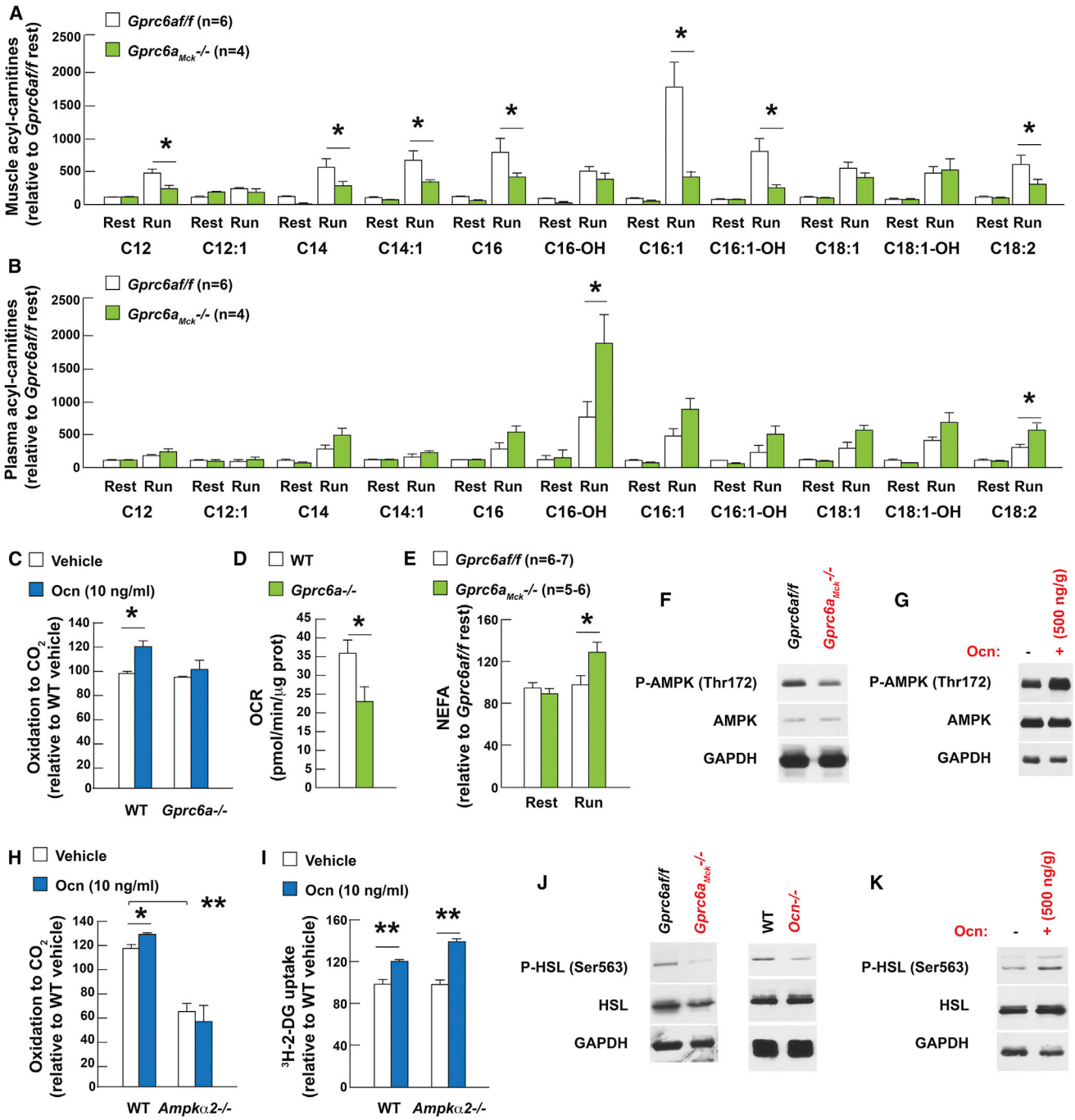

Figure 4. Osteocalcin Signaling in Myofibers Favors FA Utilization during Exercise

(A and B) (A) Acylcarnitine levels in quadriceps muscles and (B) plasma of 3-month-old *Gprc6a*$^{f/f}$ and *Gprc6a*$_{Mck}$$^{-/-}$ mice at rest and after exercise.

(C) ^{14}C-oleate oxidation in WT and *Gprc6a*$^{-/-}$ myotubes treated with osteocalcin (Ocn).

(D) Oxygen consumption rate (OCR) in myofibers cultured in Krebs-Ringer HEPES buffer with 3 mM oleic acid.

(E) Plasma NEFA levels in 3-month-old *Gprc6a*$^{f/f}$ and *Gprc6a*$_{Mck}$$^{-/-}$ mice at rest and after exercise.

(F and G) (F) Western blot analysis after exercise of AMPK phosphorylation (Thr172) in tibialis muscles of 3-month-old *Gprc6a*$^{f/f}$ and *Gprc6a*$_{Mck}$$^{-/-}$ mice or (G) of 15-month-old WT mice injected with Ocn.

(H) ^{14}C-oleate oxidation in WT and *Ampkα2*$^{-/-}$ myotubes treated with Ocn.

(I) Uptake of ^{3}H-2-deoxyglucose (^{3}H-2-DG) in WT and *Ampkα2*$^{-/-}$ myotubes treated with vehicle or Ocn.

(J and K) (J) Western blot analysis after exercise of HSL phosphorylation (Ser563) in tibialis muscles of 3-month-old *Gprc6a*$^{f/f}$, *Gprc6a*$_{Mck}$$^{-/-}$, WT, and *Ocn*$^{-/-}$ mice, and (K) 15-month-old WT mice injected with Ocn.

(Exercise refers to 40 min running at 30 cm/s on a treadmill.) All data are presented as mean ± SEM.

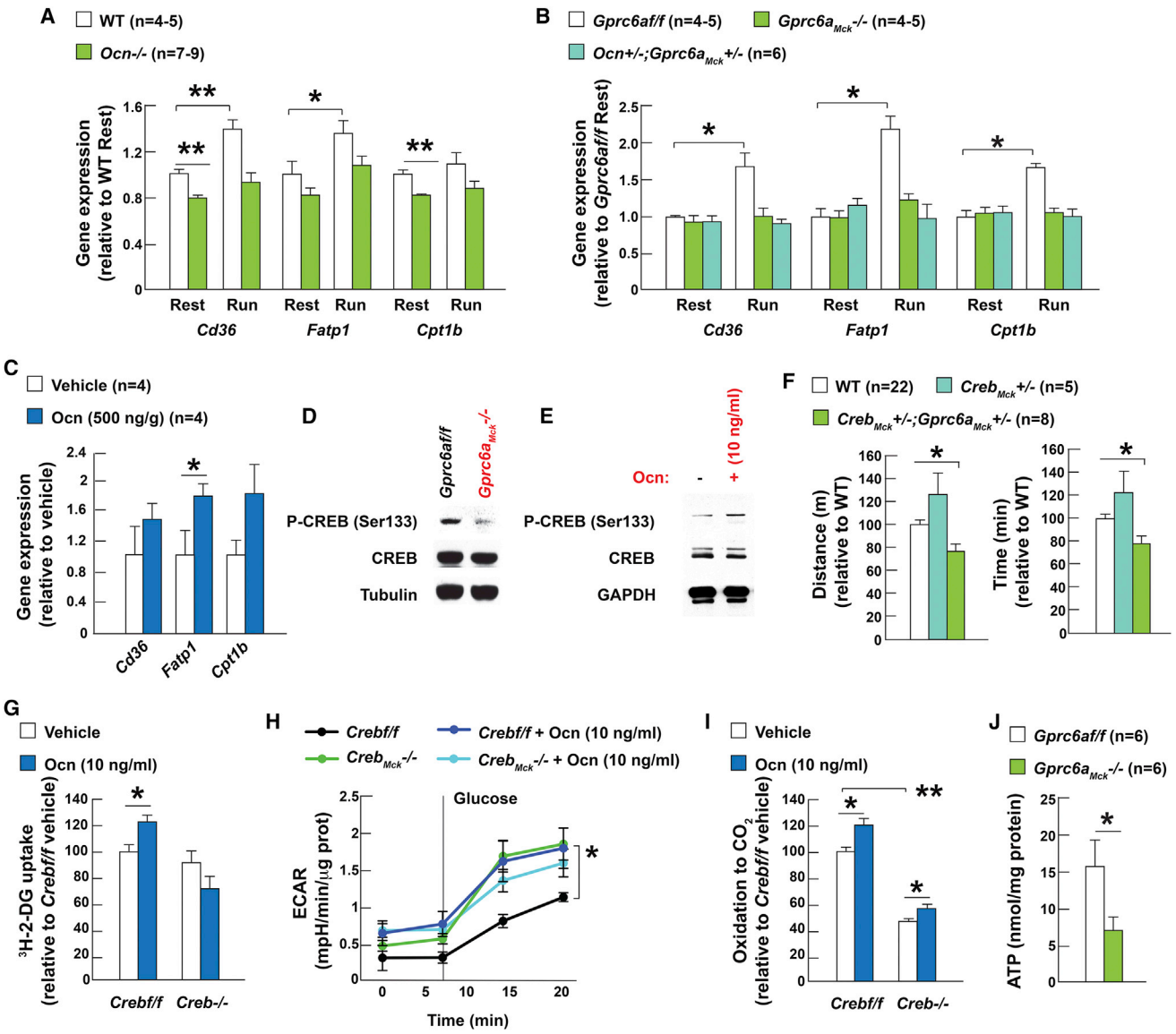

Figure 5. Osteocalcin Signaling in Myofibers Favors Expression of FA Transporters during Exercise

(A) *Cd36*, *Fatp1*, and *Cpt1b* expression at rest and after exercise in gastrocnemius muscles of 3-month-old WT and *Ocn*$^{-/-}$ mice.

(B and C) (B) *Cd36*, *Fatp1*, and *Cpt1b* expression at rest and after exercise in gastrocnemius muscles of 3-month-old *Gprc6a*$^{f/f}$, *Gprc6a*$_{Mck}$$^{-/-}$, and *Ocn*$^{+/-}$; *Gprc6a*$_{Mck}$$^{+/-}$ mice and (C) in gastrocnemius muscles of 15-month-old WT mice injected with vehicle or osteocalcin (Ocn).

(D and E) (D) Western blot analysis after exercise of CREB phosphorylation (Ser133) in tibialis muscles of 3-month-old *Gprc6a*$^{f/f}$ and *Gprc6a*$_{Mck}$$^{-/-}$ mice and (E) in WT myotubes treated with vehicle or Ocn.

(F) Performance during an endurance test (running on a treadmill at 30 cm/s until exhausted) of 3-month-old *Gprc6a*$_{Mck}$$^{+/-}$;*Creb*$_{Mck}$$^{+/-}$, *Creb*$_{Mck}$$^{+/-}$, and control mice.

(G) Uptake of ^{3}H-2-deoxyglucose (^{3}H-2-DG) in *Creb*$^{f/f}$ and *Creb*$^{-/-}$ myotubes treated with vehicle or Ocn.

(H) Glycolysis, determined by the extracellular acidification of the media (ECAR), in *Creb*$^{f/f}$ and *Creb*$_{Mck}$$^{-/-}$ myofibers treated with vehicle or Ocn.

(I) ^{14}C-oleate oxidation in *Creb*$^{f/f}$ and *Creb*$^{-/-}$ myotubes treated with Ocn.

(J) ATP accumulation in quadriceps muscles of 3-month-old *Gprc6a*$^{f/f}$ and *Gprc6a*$_{Mck}$$^{-/-}$ mice after exercise.

(Exercise refers to 40 min running at 30 cm/s on a treadmill.) All data are presented as mean ± SEM.

The gene whose expression was the most decreased (80%) in *Gprc6a*$_{Mck}$$^{-/-}$ muscle after exercise was the one encoding IL-6, a myokine whose circulating levels markedly rise during exercise through previously unknown mechanisms (Whitham et al., 2012) (Figure 6A). A more modest decrease of the expression of the soluble IL-6 receptor was also observed, whereas no other myokines known to influence exercise (Boström et al., 2012; Egan and Zierath, 2013; Heinemeier et al., 2007) were affected by the absence of osteocalcin signaling in myofibers during exercise (Figure S6A). We verified that *Il6* and *Il6rα* expression was significantly lower in muscles of *Gprc6a*$_{Mck}$$^{-/-}$ and *Ocn*$^{-/-}$ than in those of control mice after

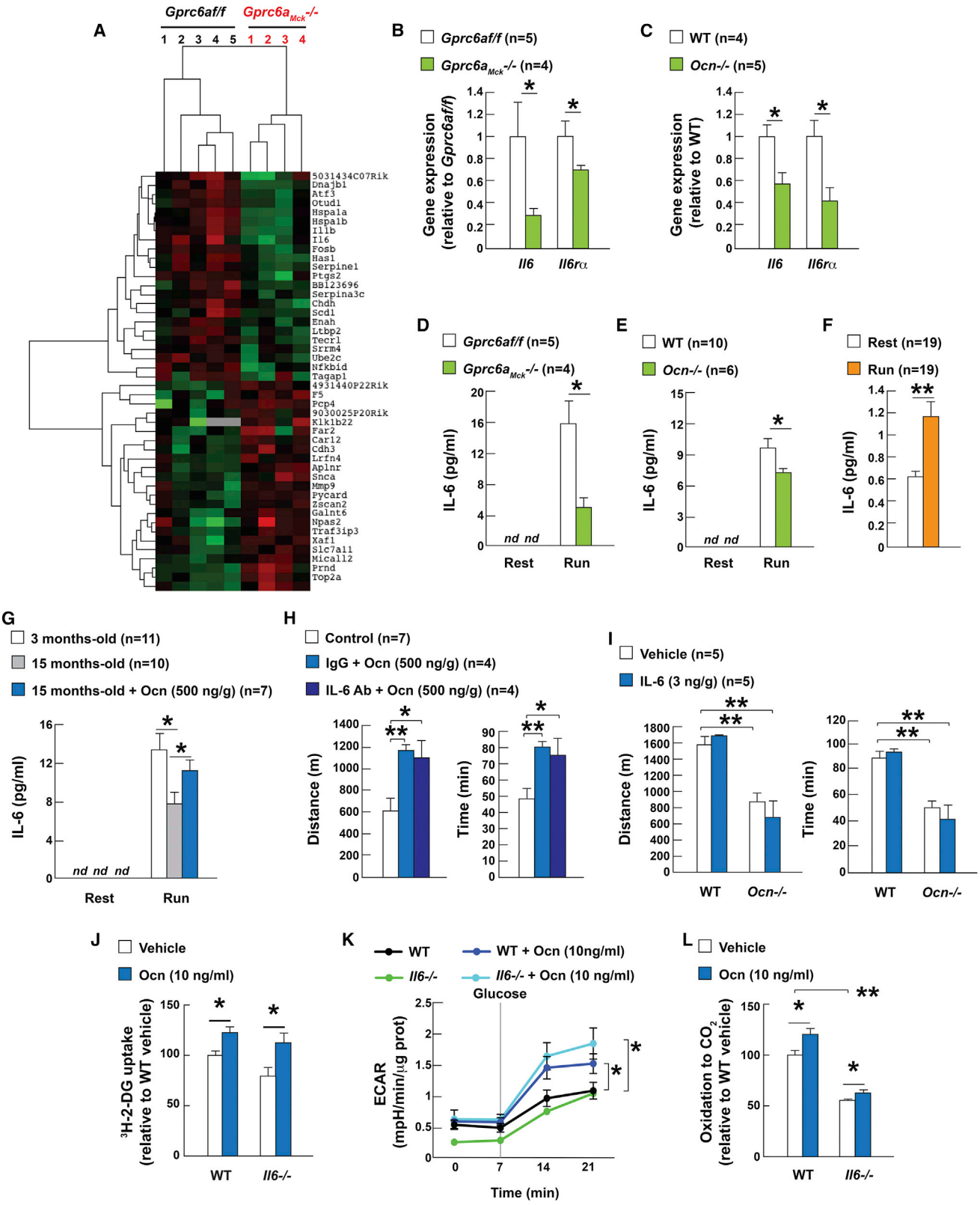

Figure 6. Osteocalcin Is Necessary for the Increase in *Interleukin-6* Expression in Muscle during Exercise

(A) RNA-seq analyses in gastrocnemius muscles of 3-month-old *Gprc6a*$^{f/f}$ and *Gprc6a*$_{Mck}$$^{-/-}$ mice after exercise.

(B and C) (B) Expression after exercise of *Il6* and *Il6rα* in gastrocnemius muscles of 3-month-old *Gprc6a*$^{f/f}$ and *Gprc6a*$_{Mck}$$^{-/-}$ and (C) WT and *Ocn*$^{-/-}$ mice.

(legend continued on next page)

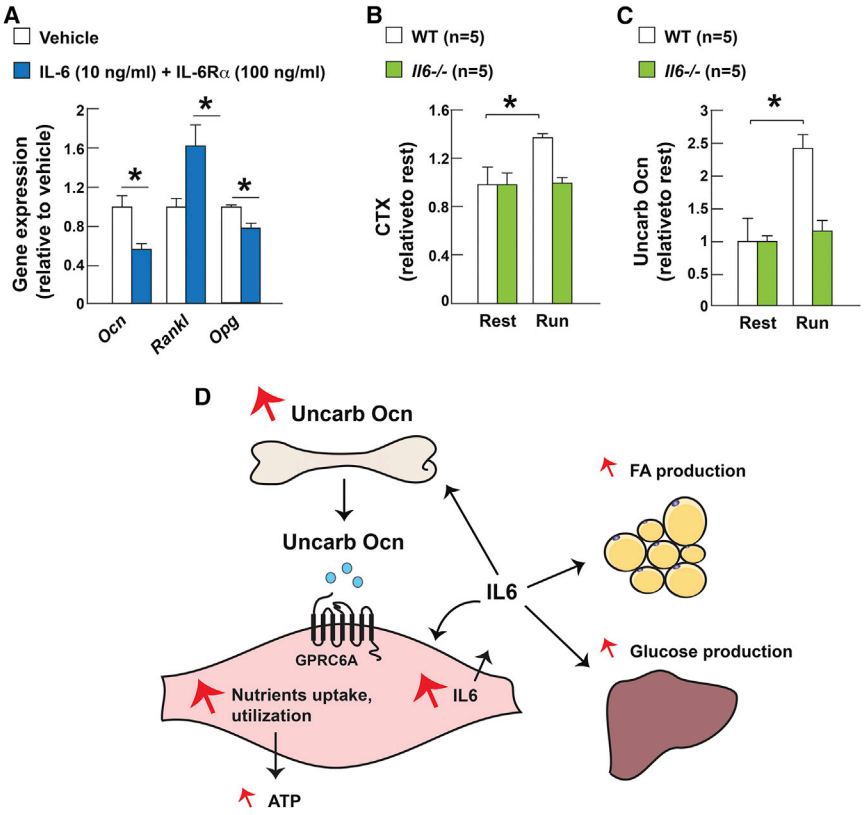

Figure 7. IL-6 Favors the Production of Active Osteocalcin during Exercise

(A) *Ocn*, *Rankl*, and *Opg* expression in osteoblasts treated with IL-6 and soluble IL-6Rα.

(B) Serum CTX levels in 2-month-old WT and *Il6*$^{-/-}$ mice after exercise.

(C) Serum undercarboxylated osteocalcin (uncarb Ocn) levels in 2-month-old WT and *Il6*$^{-/-}$ mice at rest and after exercise.

(D) Schematic representation of how osteocalcin signaling in myofibers and muscle-derived IL-6 cooperate to favor adaptation to exercise.

(Exercise refers to 40 min running at 30 cm/s on a treadmill.) All data are presented as mean ± SEM.

exercise (Figures 6B and 6C). We also observed that the rise in circulating IL-6 levels induced by exercise in control mice was blunted in *Gprc6a*$_{Mck}$$^{-/-}$ and *Ocn*$^{-/-}$ mice. Of note, IL-6 circulating levels also rise in young woman during exercise (Figures 6D–6F). Moreover, the decrease in circulating osteocalcin levels observed in 15-month-old WT mice provides an explanation for the modest increase in circulating IL-6 levels observed during exercise; indeed, exogenous osteocalcin partially restored circulating IL-6 levels in these mice during exercise (Figure 6G). These observations identify osteocalcin as a major regulator of *Il6* expression in muscle and suggest that the majority of the increase in IL-6 circulating levels observed during exercise originates from muscle.

The results presented above raise the important question of whether or not osteocalcin signaling in myofibers during exercise requires the presence of IL-6 in muscle or blood. In vivo, injection of a neutralizing antibody against IL-6 prior to exercise did not prevent the increase in exercise capacity induced by exogenous osteocalcin in WT mice, and exogenous IL-6 (3 ng/g of body weight) did not improve the exercise capacity of WT or *Ocn*$^{-/-}$ mice (Figures 6H, 6I, and S6B). Ex vivo, osteocalcin increased glucose uptake (^{3}H-2-DG uptake), glycolysis (ECAR), and FA oxidation (^{14}C-oleate oxidation) equally well in WT and *Il6*$^{-/-}$ myotubes (Figures 6J–6L). Taken together, these results show that osteocalcin signals in muscle regardless of the presence or absence of IL-6 in the general circulation or in myofibers. However, IL-6 favors adaptation to exercise through previously described mechanisms and a novel one presented below.

IL-6 Favors the Production of Bioactive Osteocalcin during Exercise

Indeed, since IL-6 has been shown to signal in bone cells (Tamura et al., 1993), we asked whether one mechanism whereby IL-6 favors adaptation to exercise may be by favoring the production of osteocalcin by osteoblasts and/or its activation by bone resorption (Ferron et al., 2010). In cell culture, IL-6 decreased the expression of *Osteocalcin* (*Ocn*) in osteoblasts but, more importantly, increased the expression of *Rankl*, a cytokine that favors osteoclast differentiation, and decreased that of *Osteoprotegerin* (*Opg*), a decoy receptor for Rankl and an inhibitor of bone resorption (Teitelbaum and Ross, 2003) (Figure 7A). These results provide one explanation for why bone resorption and circulating levels of bioactive osteocalcin significantly increase during exercise in WT mice that have high circulating levels of IL-6 at that time, but do not do so in *Il6*$^{-/-}$ mice (Figures 1A–1C, 7B, and 7C). This set of experiments reveals the existence of a feedforward regulatory loop linking the production of

(D–F) (D) Circulating IL-6 at rest and after exercise in 3-month-old *Gprc6a*$^{f/f}$ and *Gprc6a*$_{Mck}$$^{-/-}$ mice, (E) WT and *Ocn*$^{-/-}$ mice, and (F) women (45 min run on a treadmill [6.5 km/hr]).

(G) Circulating IL-6 at rest and after exercise in 3- and 15-month-old mice and 15-month-old mice treated with vehicle or osteocalcin (Ocn).

(H) Performance during an endurance test (running on a treadmill at 30 cm/s until exhausted) of 15-month-old mice treated with vehicle or Ocn and an antibody against IL-6 or a control IgG (control group includes mice treated with vehicle alone, vehicle and IL-6 antibody, and vehicle and IgG).

(I) Performance during an endurance test (running on a treadmill at 30 cm/s until exhausted) of 6-month-old WT and *Ocn*$^{-/-}$ mice treated with IL-6.

(J–L) (J) Uptake of ^{3}H-2-deoxyglucose (^{3}H-2-DG); (K) glycolysis, determined by the extracellular acidification of the media (ECAR); and (L) ^{14}C-Oleate oxidation in WT and *Il6*$^{-/-}$ myotubes treated with vehicle or osteocalcin.

(Exercise refers to 40 min running at 30 cm/s on a treadmill; nd, non-detected.) All data are presented as mean ± SEM.

osteocalcin in bone and the synthesis of IL-6 in muscle that appears to be necessary for the increase in muscle function during exercise.

DISCUSSION

This study reveals that osteocalcin signaling in myofibers is necessary to increase adaptation to exercise in part because it promotes the uptake and catabolism of glucose and FAs in myofibers, and in part because it increases the secretion by muscle during exercise of IL-6, a myokine that favors the production of bioactive osteocalcin (Figure 7D). This study also shows that osteocalcin is sufficient to reverse the decline in muscle function occurring during aging.

Osteocalcin Signaling in Myofibers Is Necessary for Adaptation to Exercise

During exercise, the uptake and catabolism of glucose and FAs in myofibers increase. The fact that insulin exerts mostly anabolic functions in muscle and that its circulating levels decrease during exercise (Saltiel and Kahn, 2001) implies that muscle function and thereby adaptation to exercise are regulated by other secreted factors that would stimulate glucose uptake into muscle, glycogen breakdown, and/or FA uptake and catabolism. Conceivably, the circulating levels of these factors would rise during exercise. It is precisely because its circulating levels double during exercise that we tested if osteocalcin is implicated in the regulation of adaptation to exercise. Analyzing mutant mouse strains lacking *Osteocalcin* and/or its receptor *Gprc6a* in a cell-specific manner showed that osteocalcin signaling in myofibers through Gprc6a is needed for muscle function during exercise. The fact that exogenous osteocalcin could not correct the poor exercise capacity of $Gprc6a_{Mck}^{-/-}$ mice and that $Ocn^{+/-}$;$Gprc6a_{Mck}^{+/-}$ mice display the same decrease in exercise capacity as $Ocn^{-/-}$ or $Gprc6a_{Mck}^{-/-}$ mice identifies osteocalcin as the main ligand of Gprc6a responsible for its regulation of muscle function and adaptation to exercise. Cell-specific and inducible deletion of *Ocn* established that this function of osteocalcin reflects an influence of bone on muscle that is not of developmental origin. This function of osteocalcin is also not secondary to its signaling in the heart. Hence, by signaling through Gprc6a in myofibers, osteocalcin is a systemic regulator of the adaptation to exercise in adult mice.

Osteocalcin Favors Uptake and Catabolism of Nutrients in Muscle during Exercise

While osteocalcin does not affect in any appreciable manner muscle contractility or mitochondrial biogenesis, it favors the uptake and utilization of nutrients in myofibers during exercise in several ways. First, osteocalcin signaling in myofibers favors the breakdown of glycogen, a major source of glucose for contracting muscles during exercise. Second, it promotes the translocation of the glucose transporter GLUT4 to the plasma membrane and thereby enhances glucose uptake and glycolysis. None of the other proposed ligands of Gprc6a increased glucose uptake and glycolysis in myofibers. Third, osteocalcin signaling in myofibers increases FA uptake and catabolism. Through these combined functions, osteocalcin signaling in myofibers provides the carbon atoms necessary to promote the activity of the TCA cycle and thereby produce the ATP that is needed to increase muscle function. That osteocalcin signaling in myofibers is important mainly during exercise is consistent with the notion that the endocrine regulation of nutrient uptake and utilization in muscle differs at rest and during exercise (Egan and Zierath, 2013). These findings do not exclude in any way the likely possibility that other molecules may contribute to the regulation of adaptation to exercise. The fact that osteocalcin signaling in myofibers increases uptake and catabolism of both glucose and FAs provides an explanation for why RER, which reflects the respective utilization of both nutrients, is not affected in $Gprc6_{Mck}^{-/-}$ mice during exercise.

A Crosstalk between Bone and Muscle Determines Adaptation to Exercise

Our study also identified IL-6, a myokine whose circulating levels rise during exercise and that enhances exercise capacity (Pedersen and Febbraio, 2012), as an osteocalcin target gene in muscle. In turn, IL-6 favors adaptation to exercise in part by signaling in bone to increase osteoclast differentiation and the generation of bioactive osteocalcin. Thus, a feedforward loop between bone and muscle promotes adaptation to exercise through at least three synergistic mechanisms: first, osteocalcin enhances the uptake and catabolism of glucose and FAs in myofibers. Second, the rise in IL-6 secretion from muscle during exercise, triggered by osteocalcin, allows for the generation of glucose and FAs (Febbraio et al., 2004; van Hall et al., 2003). Third, IL-6, through its regulation of bone resorption, increases the production of bioactive osteocalcin (Figure 7D). This model does not exclude the likely possibility that osteocalcin and IL-6 favor adaptation to exercise through additional mechanisms.

Osteocalcin Signaling in Muscle Can Reverse the Age-Related Decline in Muscle Function

The fact that osteocalcin is necessary for adaptation to exercise, together with the precipitous decline of its circulating levels before midlife in all species tested, raised the question of whether osteocalcin could also be sufficient to reverse the decline in muscle function that is caused by aging. Whether administered acutely or chronically, exogenous osteocalcin increased the exercise capacity of 3-month-old WT mice and restored the exercise capacity of 9-, 12-, and even 15-month-old mice to that of 3-month-old ones. This ability of osteocalcin to reverse the age-related decline in exercise capacity in mice requires that this hormone signal in myofibers. These results identify osteocalcin signaling in myofibers as a novel and powerful means to fight the age-related decline in muscle function. Given the growing number of molecules proposed to affect muscle functions (Baskin et al., 2015), it will be important to determine if osteocalcin synergizes with some of them to favor adaptation to exercise.

EXPERIMENTAL PROCEDURES

Animal and Human Studies

$Ocn^{-/-}$ mice were maintained on a 129-Sv genetic background; $Ocn_{Osb}^{-/-}$, $Gprc6a_{Mck}^{-/-}$, $Gprc6a_{Myh6}^{-/-}$, $Creb_{Mck}^{-/-}$, $Ocn^{+/-}$;$Gprc6a_{Mck}^{+/-}$, and $Gprc6a_{Mck}^{+/-}$;$Creb_{Mck}^{+/-}$ mice (all procedures involving mice were approved by CUMC IACUC and conform to the relevant regulatory standards) on a 129-Sv/C57/BL6 mixed genetic background; and $Il6^{-/-}$ (Jackson Laboratories)

mice on a C57/BL6 genetic background. Littermates were used as controls in all experiments. Mice genotypes were determined by PCR. Generations of *Ocn* and *Gprc6a* conditional alleles have been described (Oury et al., 2011, 2013). For exercise studies, all mice were trained to run on a treadmill for 3 days (10 min/day, increasing speed from 10 to 17 cm/s, and an electric shock at 1 mA to trigger running). Exercise tests were performed on mice fed ad libitum at 2–6 p.m. The day of the test, mice were acclimated to the treadmill for 5 min, followed by 10 min running at a constant speed (17 cm/s), followed by a gradual speed increase up to 30 cm/s. Then mice run either until exhaustion to determine endurance capacity, or for 40 min. A gradual speed increase test was performed to determine the maximal VO_2 during exercise: mice were acclimated to the treadmill for 5 min, followed by 1 min running at 5 cm/s, followed by a gradual speed increase (3 cm/s every minute) until exhaustion, defined as the number of times a mouse fell off onto the electric grid during 1 min out of 15. For all biochemical and metabolic analyses, blood/tissues were collected and processed either at rest or at the end of a 40 min run (30 cm/s). i.p. injections of exogenous osteocalcin or IL-6 (Sigma) were performed immediately before exercise. To neutralize IL-6, 500 μg of a neutralizing antibody (R&D, #MAB206) (Pedersen et al., 2016) was administered i.p. 1 hr before exercise. Osteocalcin was synthetized as previously described (Oury et al., 2013).

Rhesus monkeys (*Macaca mulatta*) were housed as described in Supplemental Information at the NIH Animal Center. All procedures and animal care were conducted in accordance with the NIH Guide for the Care and Use of Laboratory Animals. Human healthy volunteers were used to assay osteocalcin (Elecsys, Roche Diagnosis) across lifespan (see Supplemental Information). Human studies were approved by local ethic comittee of Lyon University, France.

Energy Metabolism Studies

Glucose and insulin tolerance tests were performed as described (Lee et al., 2007). Ex vivo glucose uptake in EDL and soleus muscles was measured as described (Brüning et al., 1998) with minor modifications (see Supplemental Information). For in vivo glucose uptake, a bolus of 2-deoxy-d-[^{3}H]glucose (^{3}H-2-DG) (10 μCi) was administered before running (40 min at 30 cm/s). ^{3}H-2-DG and ^{3}H-2-DG-6-P content in muscle was determined by liquid scintillation counter and normalized to muscle weight (see Supplemental Information). Glucose uptake and FA oxidation in myotubes were assayed as described (Sebastián et al., 2007). GLUT4 translocation was determined by optic microscopy as described (Zeigerer et al., 2002) (see Supplemental Information). OCR and extracellular acidification of the media (ECAR) in myofibers were measured using an XF24 Seahorse analyzer (Seahorse Biosciences) (see Supplemental Information). To analyze mitochondrial function, myofibers were treated sequentially with oligomycin (10 μg/mL), FCCP (200 μM), and rotenone (0.2 μM). OCR was recorded following administration of each of them.

Metabolite profiling was done at the Einstein Stable Isotope and Metabolomics Core Facility. Metabolites from freeze-clamped skeletal muscles were extracted, derivatized, and run for GC-TOFMS analysis (Qiu et al., 2014). Liquid chromatography-tandem mass spectrometry (LC-MS/MS) analysis was used to quantify glycolytic and TCA cycle metabolites (Serasinghe et al., 2015). The Biocrates Absolute*IDQ* p180 kit (Wang-Sattler et al., 2012) was used to quantify acylcarnitines by LC-MS/MS in plasma and muscle (see Supplemental Information). ^{13}C-glucose tracer analyses were done at CASE Mouse Metabolic Phenotyping Center (see Supplemental Information). ATP was measured using commercial kit (Abcam). Ex vivo analyses of muscle contractility and resistance to fatigue were performed as detailed in Supplemental Information.

Biochemistry and Molecular Biology

Serum osteocalcin, PINP, CTX, IL-6, and insulin levels were measured using ELISA assays. Blood glucose level was measured using an Accu-Check glucometer. Cyclic AMP accumulation was measured using a commercial kit (R&D). For gene expression, 1 μg of total RNA was reverse transcribed into cDNA. qPCR analyses were performed using a SYBER green master mix (Applied Biosciences) and a CFX-Connect real-time PCR (Bio-Rad). Relative expression levels of each gene were normalized to the one of *Hprt* or *Gapdh*. The genome-wide differential expression of $Gprc6a_{Mck}^{-/-}$ versus $Gprc6a^{f/f}$ in muscle was measured by RNA sequencing (RNA-seq) (see Supplemental Information). For western blot analyses, protein extracts were separated in 8% acrylamide/Bis-acrylamide (Bio-Rad) gels and transferred to nitrocellulose membranes that were blotted using specific antibodies. For in situ hybridization, muscles were frozen in liquid N_2-cooled methylbutane. Samples were sectioned at 10 μm using a cryostat. In situ hybridization was performed with a DIG-labeled riboprobe. Mitochondria histomorphometry and enzyme histochemistry were performed following standard protocols (see Supplemental Information).

Cell Culture

Culture of skeletal muscle myoblasts was performed as described (Gharaibeh et al., 2008), using 15- to 20-day-old mice. Myoblasts were differentiated into myotubes for 3–4 days in a medium containing 5% horse serum. For in vitro gene inactivation of *Gprc6a* and *Il6*, myoblasts from either WT or mutant littermate mice were isolated and differentiated into myotubes. For in vitro gene inactivation of *Creb* and *Ampkα2*, floxed myoblasts were isolated from mice, then divided into two groups and infected with either empty or Cre-expressing adenovirus for 2 days (University of Iowa). Muscle fibers from flexor digitorum brevis muscle were isolated from 2- to 3-month-old WT or mutant mice. Muscles were dissociated with DMEM 2% collagenase for 2 hr at 37°C in 5% CO_2 incubator. Muscle fibers were disaggregated from the tissue using a wide bore pipet and plated on matrigel-coated plates at approximately 50% confluence (see Supplemental Information). Myofibers were used after overnight incubation. Osteoblast culture was performed as described (Ducy and Karsenty, 1995).

Statistics

All data are presented as mean ± SEM. Statistical analyses were performed using unpaired, two-tailed Student's t test for comparison between two groups and ANOVA test for experiments involving more than two groups. For all experiments, $^*p \leq 0.05$, $^{**}p \leq 0.005$.

SUPPLEMENTAL INFORMATION

Supplemental Information includes Supplemental Experimental Procedures and six figures and can be found with this article online at http://dx.doi.org/10.1016/j.cmet.2016.05.004.

AUTHOR CONTRIBUTIONS

P.M. and G.K. conceived the study; P.M., K.L., M.F., J.W., and M.G.-D. performed most experiments; I.K. performed metabolomics studies; C.C., J.B., and P.S. performed human studies; A.L. analyzed muscle contractility; Y.C. and R.N.K. analyzed heart function; S.J.M., J.A.M., and R.dC. provided mice and monkey serum samples; C.T. and T.E.M. analyzed GLUT4 translocation; M.P. analyzed tracer analyses; and P.M. and G.K. wrote the manuscript.

ACKNOWLEDGMENTS

We thank Drs. C. Cosentino, P. Ducy, L. Herrero, M. Hussain, R. Sellers, D. Serra, and E. Sornay-Rendu for advice or reagents, and Dr. M. McKee for electronic microscopy analyses. This work was supported by NIH grants 5RO1AR045548, PO1AG032959 (G.K.), P60DK020541 (I.K.), RO1HL60665 (R.N.K.), and U24DK76174 (M.P.); the Wilf Family Foundation (R.N.K.); an Ellison Senior Scholar Award (G.K.); an EMBO postdoctoral fellowship (K.L.); and the Intramural Research Program of the National Institute on Aging (R.dC., S.J.M., and J.A.M.).

Received: December 17, 2015
Revised: April 4, 2016
Accepted: May 17, 2016
Published: June 14, 2016; corrected online: December 23, 2016

REFERENCES

Baskin, K.K., Winders, B.R., and Olson, E.N. (2015). Muscle as a "mediator" of systemic metabolism. Cell Metab. *21*, 237–248.

Boström, P., Wu, J., Jedrychowski, M.P., Korde, A., Ye, L., Lo, J.C., Rasbach, K.A., Boström, E.A., Choi, J.H., Long, J.Z., et al. (2012). A PGC1-α-dependent myokine that drives brown-fat-like development of white fat and thermogenesis. Nature *481*, 463–468.

Brüning, J.C., Michael, M.D., Winnay, J.N., Hayashi, T., Hörsch, D., Accili, D., Goodyear, L.J., and Kahn, C.R. (1998). A muscle-specific insulin receptor knockout exhibits features of the metabolic syndrome of NIDDM without altering glucose tolerance. Mol. Cell *2*, 559–569.

Catoire, M., and Kersten, S. (2015). The search for exercise factors in humans. FASEB J. *29*, 1615–1628.

Coderre, L., Kandror, K.V., Vallega, G., and Pilch, P.F. (1995). Identification and characterization of an exercise-sensitive pool of glucose transporters in skeletal muscle. J. Biol. Chem. *270*, 27584–27588.

Da Cruz, S., Parone, P.A., Lopes, V.S., Lillo, C., McAlonis-Downes, M., Lee, S.K., Vetto, A.P., Petrosyan, S., Marsala, M., Murphy, A.N., et al. (2012). Elevated PGC-1α activity sustains mitochondrial biogenesis and muscle function without extending survival in a mouse model of inherited ALS. Cell Metab. *15*, 778–786.

Deshmukh, A., Coffey, V.G., Zhong, Z., Chibalin, A.V., Hawley, J.A., and Zierath, J.R. (2006). Exercise-induced phosphorylation of the novel Akt substrates AS160 and filamin A in human skeletal muscle. Diabetes *55*, 1776–1782.

Ducy, P., and Karsenty, G. (1995). Two distinct osteoblast-specific cis-acting elements control expression of a mouse osteocalcin gene. Mol. Cell. Biol. *15*, 1858–1869.

Egan, B., and Zierath, J.R. (2013). Exercise metabolism and the molecular regulation of skeletal muscle adaptation. Cell Metab. *17*, 162–184.

Febbraio, M.A., Hiscock, N., Sacchetti, M., Fischer, C.P., and Pedersen, B.K. (2004). Interleukin-6 is a novel factor mediating glucose homeostasis during skeletal muscle contraction. Diabetes *53*, 1643–1648.

Ferron, M., Wei, J., Yoshizawa, T., Del Fattore, A., DePinho, R.A., Teti, A., Ducy, P., and Karsenty, G. (2010). Insulin signaling in osteoblasts integrates bone remodeling and energy metabolism. Cell *142*, 296–308.

Gharaibeh, B., Lu, A., Tebbets, J., Zheng, B., Feduska, J., Crisan, M., Péault, B., Cummins, J., and Huard, J. (2008). Isolation of a slowly adhering cell fraction containing stem cells from murine skeletal muscle by the preplate technique. Nat. Protoc. *3*, 1501–1509.

Gibala, M.J., MacLean, D.A., Graham, T.E., and Saltin, B. (1998). Tricarboxylic acid cycle intermediate pool size and estimated cycle flux in human muscle during exercise. Am. J. Physiol. *275*, E235–E242.

Handschin, C., and Spiegelman, B.M. (2008). The role of exercise and PGC1alpha in inflammation and chronic disease. Nature *454*, 463–469.

Hawley, J.A., Hargreaves, M., Joyner, M.J., and Zierath, J.R. (2014). Integrative biology of exercise. Cell *159*, 738–749.

Heinemeier, K.M., Olesen, J.L., Schjerling, P., Haddad, F., Langberg, H., Baldwin, K.M., and Kjaer, M. (2007). Short-term strength training and the expression of myostatin and IGF-I isoforms in rat muscle and tendon: differential effects of specific contraction types. J. Appl. Physiol. *102*, 573–581.

Jensen, T.E., Rose, A.J., Jørgensen, S.B., Brandt, N., Schjerling, P., Wojtaszewski, J.F., and Richter, E.A. (2007). Possible CaMKK-dependent regulation of AMPK phosphorylation and glucose uptake at the onset of mild tetanic skeletal muscle contraction. Am. J. Physiol. Endocrinol. Metab. *292*, E1308–E1317.

Karsenty, G., and Olson, E.N. (2016). Bone and muscle endocrine functions: unexpected paradigms of inter-organ communication. Cell *164*, 1248–1256.

Koves, T.R., Li, P., An, J., Akimoto, T., Slentz, D., Ilkayeva, O., Dohm, G.L., Yan, Z., Newgard, C.B., and Muoio, D.M. (2005). Peroxisome proliferator-activated receptor-gamma co-activator 1alpha-mediated metabolic remodeling of skeletal myocytes mimics exercise training and reverses lipid-induced mitochondrial inefficiency. J. Biol. Chem. *280*, 33588–33598.

Lee, N.K., Sowa, H., Hinoi, E., Ferron, M., Ahn, J.D., Confavreux, C., Dacquin, R., Mee, P.J., McKee, M.D., Jung, D.Y., et al. (2007). Endocrine regulation of energy metabolism by the skeleton. Cell *130*, 456–469.

Lehninger, A.L., Nelson, D.L., and Cox, M.M. (2000). Lehninger Principles of Biochemistry, Third Edition (Worth Publishers).

Lopez-Ilasaca, M., Crespo, P., Pellici, P.G., Gutkind, J.S., and Wetzker, R. (1997). Linkage of G protein-coupled receptors to the MAPK signaling pathway through PI 3-kinase gamma. Science *275*, 394–397.

Lund, S., Holman, G.D., Schmitz, O., and Pedersen, O. (1995). Contraction stimulates translocation of glucose transporter GLUT4 in skeletal muscle through a mechanism distinct from that of insulin. Proc. Natl. Acad. Sci. USA *92*, 5817–5821.

Neufer, P.D., Bamman, M.M., Muoio, D.M., Bouchard, C., Cooper, D.M., Goodpaster, B.H., Booth, F.W., Kohrt, W.M., Gerszten, R.E., Mattson, M.P., et al. (2015). Understanding the cellular and molecular mechanisms of physical activity-induced health benefits. Cell Metab. *22*, 4–11.

Novotny, S.A., Warren, G.L., and Hamrick, M.W. (2015). Aging and the muscle-bone relationship. Physiology (Bethesda) *30*, 8–16.

O'Neill, H.M., Lally, J.S., Galic, S., Thomas, M., Azizi, P.D., Fullerton, M.D., Smith, B.K., Pulinilkunnil, T., Chen, Z., Samaan, M.C., et al. (2014). AMPK phosphorylation of ACC2 is required for skeletal muscle fatty acid oxidation and insulin sensitivity in mice. Diabetologia *57*, 1693–1702.

Oury, F., Sumara, G., Sumara, O., Ferron, M., Chang, H., Smith, C.E., Hermo, L., Suarez, S., Roth, B.L., Ducy, P., and Karsenty, G. (2011). Endocrine regulation of male fertility by the skeleton. Cell *144*, 796–809.

Oury, F., Khrimian, L., Denny, C.A., Gardin, A., Chamouni, A., Goeden, N., Huang, Y.Y., Lee, H., Srinivas, P., Gao, X.B., et al. (2013). Maternal and offspring pools of osteocalcin influence brain development and functions. Cell *155*, 228–241.

Overmyer, K.A., Evans, C.R., Qi, N.R., Minogue, C.E., Carson, J.J., Chermside-Scabbo, C.J., Koch, L.G., Britton, S.L., Pagliarini, D.J., Coon, J.J., and Burant, C.F. (2015). Maximal oxidative capacity during exercise is associated with skeletal muscle fuel selection and dynamic changes in mitochondrial protein acetylation. Cell Metab. *21*, 468–478.

Partridge, L., and Gems, D. (2002). Mechanisms of ageing: public or private? Nat. Rev. Genet. *3*, 165–175.

Pedersen, B.K., and Febbraio, M.A. (2012). Muscles, exercise and obesity: skeletal muscle as a secretory organ. Nat. Rev. Endocrinol. *8*, 457–465.

Pedersen, L., Idorn, M., Olofsson, G.H., Lauenborg, B., Nookaew, I., Hansen, R.H., Johannesen, H.H., Becker, J.C., Pedersen, K.S., Dethlefsen, C., et al. (2016). Voluntary running suppresses tumor growth through epinephrine- and IL-6-dependent NK cell mobilization and redistribution. Cell Metab. *23*, 554–562.

Qiu, Y., Cai, G., Zhou, B., Li, D., Zhao, A., Xie, G., Li, H., Cai, S., Xie, D., Huang, C., et al. (2014). A distinct metabolic signature of human colorectal cancer with prognostic potential. Clin. Cancer Res. *20*, 2136–2146.

Sahlin, K., Katz, A., and Broberg, S. (1990). Tricarboxylic acid cycle intermediates in human muscle during prolonged exercise. Am. J. Physiol. *259*, C834–C841.

Saltiel, A.R., and Kahn, C.R. (2001). Insulin signalling and the regulation of glucose and lipid metabolism. Nature *414*, 799–806.

Saltiel, A.R., and Pessin, J.E. (2002). Insulin signaling pathways in time and space. Trends Cell Biol. *12*, 65–71.

Sebastián, D., Herrero, L., Serra, D., Asins, G., and Hegardt, F.G. (2007). CPT I overexpression protects L6E9 muscle cells from fatty acid-induced insulin resistance. Am. J. Physiol. Endocrinol. Metab. *292*, E677–E686.

Serasinghe, M.N., Wieder, S.Y., Renault, T.T., Elkholi, R., Asciolla, J.J., Yao, J.L., Jabado, O., Hoehn, K., Kageyama, Y., Sesaki, H., and Chipuk, J.E. (2015). Mitochondrial division is requisite to RAS-induced transformation and targeted by oncogenic MAPK pathway inhibitors. Mol. Cell *57*, 521–536.

Stahl, A., Gimeno, R.E., Tartaglia, L.A., and Lodish, H.F. (2001). Fatty acid transport proteins: a current view of a growing family. Trends Endocrinol. Metab. *12*, 266–273.

Tamura, T., Udagawa, N., Takahashi, N., Miyaura, C., Tanaka, S., Yamada, Y., Koishihara, Y., Ohsugi, Y., Kumaki, K., Taga, T., et al. (1993). Soluble interleukin-6 receptor triggers osteoclast formation by interleukin 6. Proc. Natl. Acad. Sci. USA *90*, 11924–11928.

Teitelbaum, S.L., and Ross, F.P. (2003). Genetic regulation of osteoclast development and function. Nat. Rev. Genet. *4*, 638–649.

van Hall, G., Steensberg, A., Sacchetti, M., Fischer, C., Keller, C., Schjerling, P., Hiscock, N., Møller, K., Saltin, B., Febbraio, M.A., and Pedersen, B.K. (2003). Interleukin-6 stimulates lipolysis and fat oxidation in humans. J. Clin. Endocrinol. Metab. *88*, 3005–3010.

Wang-Sattler, R., Yu, Z., Herder, C., Messias, A.C., Floegel, A., He, Y., Heim, K., Campillos, M., Holzapfel, C., Thorand, B., et al. (2012). Novel biomarkers for pre-diabetes identified by metabolomics. Mol. Syst. Biol. *8*, 615.

Watt, M.J., and Spriet, L.L. (2010). Triacylglycerol lipases and metabolic control: implications for health and disease. Am. J. Physiol. Endocrinol. Metab. *299*, E162–E168.

Whitham, M., Chan, M.H., Pal, M., Matthews, V.B., Prelovsek, O., Lunke, S., El-Osta, A., Broenneke, H., Alber, J., Brüning, J.C., et al. (2012). Contraction-induced interleukin-6 gene transcription in skeletal muscle is regulated by c-Jun terminal kinase/activator protein-1. J. Biol. Chem. *287*, 10771–10779.

Zeigerer, A., Lampson, M.A., Karylowski, O., Sabatini, D.D., Adesnik, M., Ren, M., and McGraw, T.E. (2002). GLUT4 retention in adipocytes requires two intracellular insulin-regulated transport steps. Mol. Biol. Cell *13*, 2421–2435.

Zierath, J.R., and Wallberg-Henriksson, H. (2015). Looking ahead perspective: where will the future of exercise biology take us? Cell Metab. *22*, 25–30.

Cell Metabolism, Volume *23*

Supplemental Information

Osteocalcin Signaling in Myofibers Is Necessary and Sufficient for Optimum Adaptation to Exercise

Paula Mera, Kathrin Laue, Mathieu Ferron, Cyril Confavreux, Jianwen Wei, Marta Galán-Díez, Alain Lacampagne, Sarah J. Mitchell, Julie A. Mattison, Yun Chen, Justine Bacchetta, Pawel Szulc, Richard N. Kitsis, Rafael de Cabo, Richard A. Friedman, Christopher Torsitano, Timothy E. McGraw, Michelle Puchowicz, Irwin Kurland, and Gerard Karsenty

Supplemental Figures

Figure S1

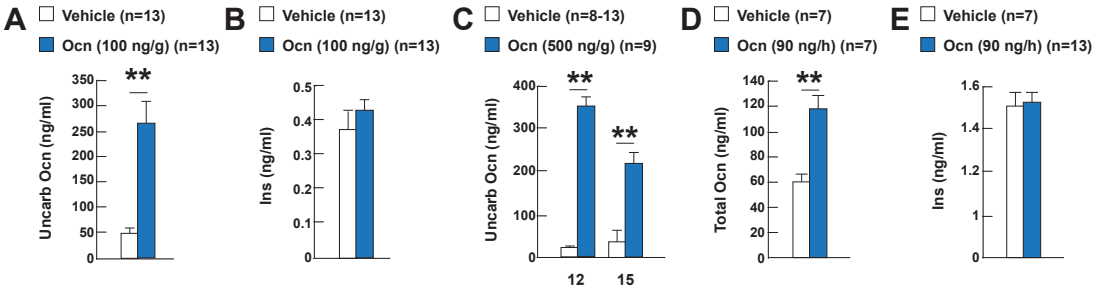

Figure S2

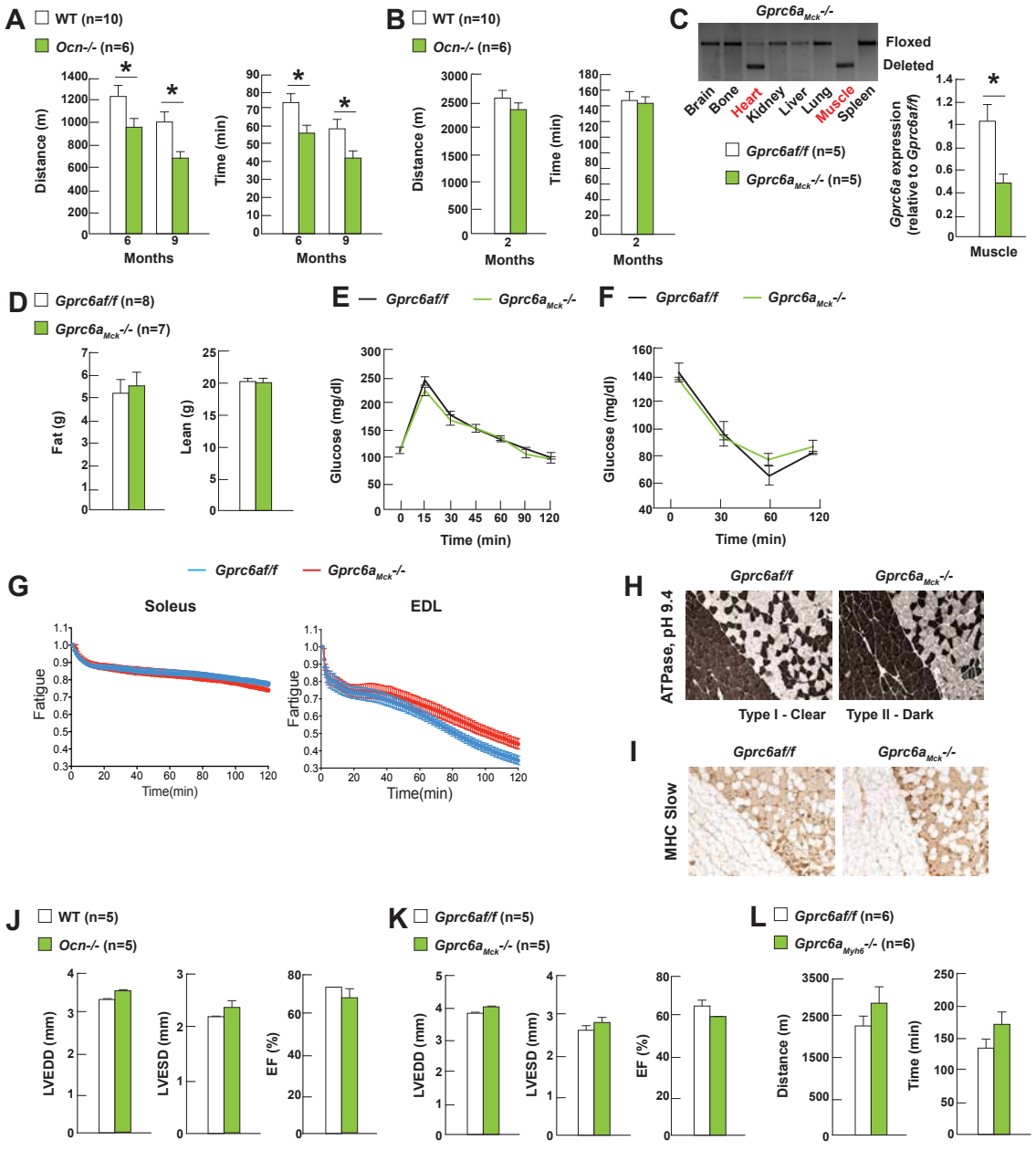
A
WT (n=10)
Ocn-/- (n=6)
Distance (m)
Time (min)
Months
B
WT (n=10)
Ocn-/- (n=6)
Distance (m)
Time (min)
Months
C
Gprc6a Mck-/-
Floxed
Deleted
Brain
Bone
Heart
Kidney
Liver
Lung
Muscle
Spleen
Gprc6af/f (n=5)
Gprc6a Mck-/- (n=5)
Gprc6a expression (relative to Gprc6af/f)
Muscle
D
Gprc6af/f (n=8)
Gprc6a Mck-/- (n=7)
Fat (g)
Lean (g)
E
Gprc6af/f
Gprc6a Mck-/-
Glucose (mg/dl)
Time (min)
F
Gprc6af/f
Gprc6a Mck-/-
Glucose (mg/dl)
Time (min)
G
Gprc6af/f
Gprc6a Mck-/-
Soleus
EDL
Fatigue
Time(min)
H
Gprc6af/f
Gprc6a Mck-/-
ATPase, pH 9.4
Type I - Clear
Type II - Dark
I
Gprc6af/f
Gprc6a Mck-/-
MHC Slow
J
WT (n=5)
Ocn-/- (n=5)
LVEDD (mm)
LVESD (mm)
EF (%)
K
Gprc6af/f (n=5)
Gprc6a Mck-/- (n=5)
LVEDD (mm)
LVESD (mm)
EF (%)
L
Gprc6af/f (n=6)
Gprc6a Myh6-/- (n=6)
Distance (m)
Time (min)

Figure S3

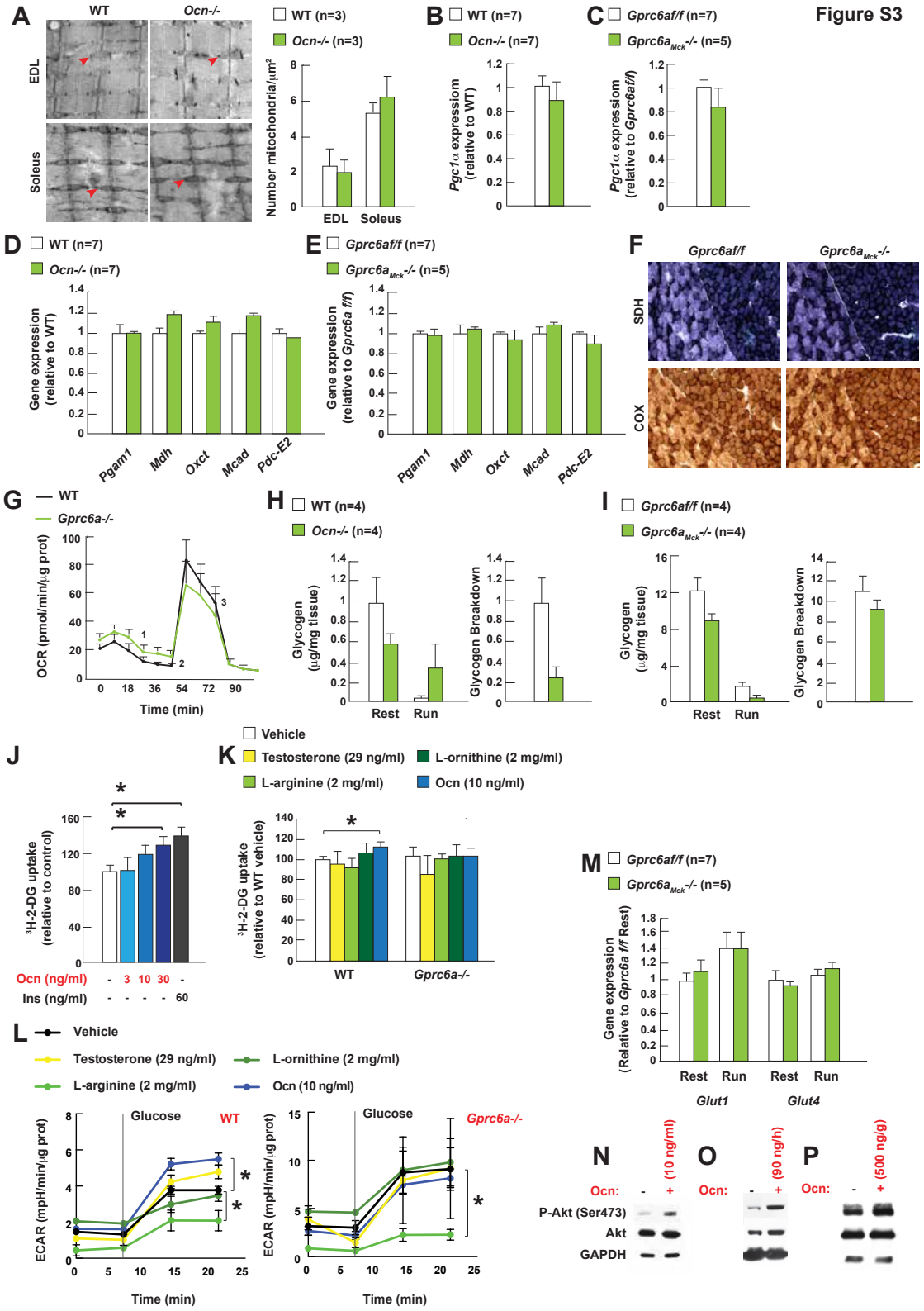
A
WT
Ocn-/-
EDL
Soleus
WT (n=3)
Ocn-/- (n=3)
Number mitochondria/μm²
EDL
Soleus
B
WT (n=7)
Ocn-/- (n=7)
Pgc1α expression (relative to WT)
C
Gprc6af/f (n=7)
Gprc6aMck-/- (n=5)
Pgc1α expression (relative to Gprc6af/f)
D
WT (n=7)
Ocn-/- (n=7)
Gene expression (relative to WT)
Pgam1
Mdh
Oxct
Mcad
Pdc-E2
E
Gprc6af/f (n=7)
Gprc6aMck-/- (n=5)
Gene expression (relative to Gprc6a f/f)
F
Gprc6af/f
Gprc6aMck-/-
SDH
COX
G
WT
Gprc6a-/-
OCR (pmol/min/μg prot)
Time (min)
H
WT (n=4)
Ocn-/- (n=4)
Glycogen (μg/mg tissue)
Glycogen Breakdown
Rest
Run
I
Gprc6af/f (n=4)
Gprc6aMck-/- (n=4)
J
3H-2-DG uptake (relative to control)
Ocn (ng/ml)
Ins (ng/ml)
K
Vehicle
Testosterone (29 ng/ml)
L-ornithine (2 mg/ml)
L-arginine (2 mg/ml)
Ocn (10 ng/ml)
3H-2-DG uptake (relative to WT vehicle)
WT
Gprc6a-/-
L
Vehicle
Testosterone (29 ng/ml)
L-ornithine (2 mg/ml)
L-arginine (2 mg/ml)
Ocn (10 ng/ml)
Glucose
WT
Gprc6a-/-
ECAR (mpH/min/μg prot)
Time (min)
M
Gprc6af/f (n=7)
Gprc6aMck-/- (n=5)
Gene expression (Relative to Gprc6a f/f Rest)
Rest
Run
Glut1
Glut4
N
Ocn:
(10 ng/ml)
P-Akt (Ser473)
Akt
GAPDH
O
Ocn:
(90 ng/h)
P
Ocn:
(500 ng/g)

Figure S4

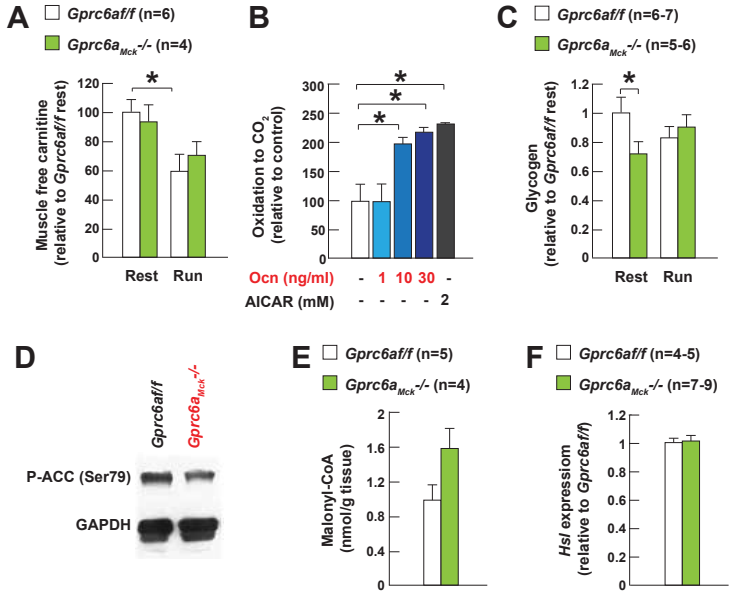
A
Gprc6af/f (n=6)
Gprc6a$_{Mck}$-/- (n=4)
Muscle free carnitine (relative to Gprc6af/f rest)
120
100
80
60
40
20
0
*
Rest
Run
B
Oxidation to CO$_2$ (relative to control)
300
250
200
150
100
50
0
*
*
*
Ocn (ng/ml) - 1 10 30 -
AICAR (mM) - - - - 2
C
Gprc6af/f (n=6-7)
Gprc6a$_{Mck}$-/- (n=5-6)
Glycogen (relative to Gprc6af/f rest)
1.2
1
0.8
0.6
0.4
0.2
0
*
Rest
Run
D
Gprc6af/f
Gprc6a$_{Mck}$-/-
P-ACC (Ser79)
GAPDH
E
Gprc6af/f (n=5)
Gprc6a$_{Mck}$-/- (n=4)
Malonyl-CoA (nmol/g tissue)
2
1.6
1.2
0.8
0.4
0
F
Gprc6af/f (n=4-5)
Gprc6a$_{Mck}$-/- (n=7-9)
Hsl expressiom (relative to Gprc6af/f)
1.2
1
0.8
0.6
0.4
0.2
0

Figure S5

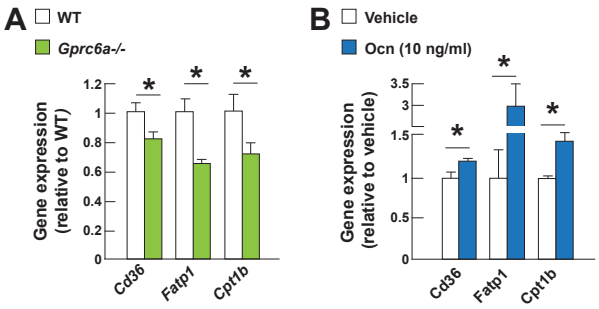
A
WT
Gprc6a-/-
Gene expression (relative to WT)
1.2
1
0.8
0.6
0.4
0.2
0
*
*
*
Cd36
Fatp1
Cpt1b
B
Vehicle
Ocn (10 ng/ml)
Gene expression (relative to vehicle)
3.5
3
1.5
1
0.5
0
*
*
*
Cd36
Fatp1
Cpt1b

Figure S6


A
Gprc6a f/f
Gprc6a Mck -/-
1 2 3 4 5 1 2 3 4
Il6
Mstn
Bdnf
Il1r1
Dcn
Fam132b
Fndc5
Il15
B
Vehicle (n=5)
IL-6 (3 ng/g) (n=4)
IL-6 (pg/ml)
18
16
14
12
10
8
6
4
2
0
Ocn-/-

Supplemental Figure Legends

Figure S1. Related to Figure 1. Regulation of circulating osteocalcin levels by exercise and age.

A. Serum undercarboxylated osteocalcin (uncarb Ocn) levels in 3 month-old WT mice injected with vehicle or Ocn immediately before running.

B. Serum insulin (Ins) levels in 3 month-old WT mice injected with vehicle or Ocn immediately before running.

C. Serum uncarb Ocn levels in 12 and 15 month-old WT mice injected with vehicle or Ocn immediately before running.

D. Serum total Ocn and **E**. Ins levels in 10 month-old WT mice treated with Ocn for 28 days.

Figure S2. Related to Figure 2. Osteocalcin signaling in myofibers is necessary for adaptation to exercise.

A. Performance during an endurance test (running on a treadmill at 30cm/s until exhausted) of 6 and 9 month-old *Ocn-/-* and WT mice and **B**. 2 month-old *Ocn-/-* and WT mice.

C. PCR analyses of *Gprc6a* deletion in various tissues in *Gprc6a*$_{Mck}$*-/-* mice and qPCR analyses of *Gprc6a* expression in gastrocnemius muscle of *Gprc6a*$_{Mck}$*-/-* and control mice.

D. Body composition in 3 month-old *Gprc6a*$_{Mck}$*-/-* and *Gprc6af/f* mice.

E. GTT in 3 month-old *Gprc6a*$_{Mck}$*-/-* and *Gprc6af/f* mice.

F. ITT in 3 month-old *Gprc6a$_{Mck}$-/-* and *Gprc6af/f* mice.

G. Muscle contraction and resistance to fatigue in isolated soleus and EDL muscles of *Gprc6a$_{Mck}$-/-* and *Gprc6af/f* mice.

H. ATPase staining in gastrocnemius/soleus muscle of 3 month-old *Gprc6a$_{Mck}$-/-* and *Gprc6af/f* mice.

I. Myosin heavy chain (MHC) slow staining in gastrocnemius/soleus muscle of 3 month-old *Gprc6a$_{Mck}$-/-* and *Gprc6af/f* mice.

J. Heart function of 3 month-old *Ocn-/-* and WT mice and **K**. *Gprc6a$_{Mck}$-/-* and *Gprc6af/f* mice measured by echocardiograpy.

L. Performance during an endurance test (running on a treadmill at 30cm/s until exhausted) of 3 month-old *Gprc6af/f* and *Gprc6a$_{Myh6}$-/-* mice.

Figure S3. Related to Figure 3. Osteocalcin signaling in myofibers promotes uptake and utilization of glucose during exercise.

A. Mitochondria number in EDL and soleus of 3 month-old WT and *Ocn-/-* mice measured by electronic microscopy.

B. *Pgc1α* expression in *Ocn-/-* and WT mice and **C**. *Gprc6af/f* and *Gprc6a$_{Mck}$-/-* mice after exercise.

D. *Pgam1, Mdh, Oxct, Mcad and Pdc-E2* expression in *Ocn-/-* and WT and **E**. *Gprc6af/f* and *Gprc6a$_{Mck}$-/-* mice after exercise.

F. SDH and COX activities in gastrocnemius/soleus muscles of *Gprc6af/f* and *Gprc6a$_{Mck}$-/-* mice after exercise.

G. Mitochondrial respiration measured in *Gprc6a-/-* and WT myofibers after the addition of (1) oligomycing, (2) FCCP and (3) rotenone.

H. Glycogen content and breakdown in 3 month-old WT and *Ocn-/-* tibialis muscles at rest and after exercise.

I. Glycogen content and breakdown in 3 month-old *Gprc6af/f* and *Gprc6a*$_{Mck}$*-/-* liver at rest and after exercise.

J. Uptake of ^{3}H-2-deoxyglucose (^{3}H-2-DG) in WT myotubes treated with vehicle or osteocalcin (Ocn).

K. Uptake of ^{3}H-2-deoxyglucose (^{3}H-2-DG) in WT and *Gprc6a-/-* myotubes treated with vehicle, testosterone, L-arginine, L-ornithine or Ocn.

L. Glycolysis determined by the extracellular acidification of the media (ECAR), in WT and *Gprc6a-/-* myofibers treated with vehicle testosterone, L-arginine, L-ornithine or Ocn.

M. *Glut1* and *Glut4* expression in *Gprc6af/f* and *Gprc6a*$_{Mck}$*-/-* in gastrocnemius muscle at rest and after exercise.

N. Western blot analyses of Akt phosphorylation (Ser473) in WT myotubes treated with Ocn.

O. Western blot analyses after exercise of Akt phosphorylation (Ser473) in tibialis muscles of 3 month-old WT mice injected with Ocn and **P**. in tibialis muscles of 15 month-old WT mice injected with Ocn.

(Exercise refers to 40 min running at 30cm/s on a treadmill).

Figure S4. Related to Figure 4. Osteocalcin signaling in myofibers favors FAs utilization during exercise.

A. Free carnitine levels in quadriceps muscles of 3 month-old *Gprc6af/f* and *Gprc6a$_{Mck}$-/-* mice at rest and after exercise.

B. ^{14}C-Oleate oxidation in WT myotubes treated with vehicle, osteocalcin (Ocn) or AICAR as a positive control.

C. Plasma NEFAs levels in *Gprc6af/f* and *Gprc6a$_{Mck}$-/-* mice at rest and after exercise.

D. Western blot analyses after exercise of ACC phosphorylation (Ser79) in tibialis muscles of 3 month-old *Gprc6af/f* and *Gprc6a$_{Mck}$-/-* mice.

E. Malonyl-CoA levels in quadriceps muscles of 3 month-old *Gprc6af/f* and *Gprc6a$_{Mck}$-/-* mice after exercise.

F. Expression of *Hsl* in gastrocnemius muscles of 3 month-old *Gprc6af/f* and *Gprc6a$_{Mck}$-/-* mice after exercise.

(Exercise refers to 40 min running at 30cm/s on a treadmill).

Figure S5. Related to Figure 5. Osteocalcin signaling in myofibers favors expression of FAs transporters during exercise.

A. *Cd36*, *Fatp1* and *Cpt1b* expression in WT and Gprc6a-/- myotubes and **B**. WT myotubes treated with vehicle or Ocn.

Figure S6. Related to Figure 6. Osteocalcin is necessary for the increase in *Interleukin-6* expression in muscle during exercise.

A. Expression of myokines in gastrocnemius muscles of 3 month-old *Gprc6af/f* and *Gprc6a*$_{Mck}$*-/-* mice after exercise.

B. Plasma IL-6 levels in 3 month-old *Ocn-/-* mice injected with vehicle or IL-6 immediately before running.

Supplemental Experimental Procedures

Monkeys and human studies

Healthy volunteers were used to assay osteocalcin (Elecsys, Roche Diagnosis) across lifespan. For children aged 10-18, age, body mass index (kg/m^2) and Tanner's stages were recorded. Children with past or present therapy with growth hormone, corticosteroids (more than 3 months), or any chronic diseases were excluded. Adult individuals were selected using the following criteria: normal body mass index, no history of smoking, fracture, diabetes, chronic diseases and anti-osteoporotic agent usage. Young adult women were non menopausal and not pregnant. Studies were approved by local ethic comity of Lyon University, France. Comparison between groups was performed using Mann-Whitney non-parametric tests and trend was assessed using logistic regression.

Rhesus monkeys (*Macaca mulatta*) were housed at the NIH Animal Center, Poolesville, MD. Monkeys were housed individually in standard non-human primate caging on a 12h light/12h dark cycle, room temperature 78 ± 2 degrees humidity at 60 ± 20%. All monkeys had extensive visual, auditory, and olfactory but limited tactile contact with monkeys housed in the same room. Monkeys received 2 meals per day *ad libitum*. Water was always available *ad libitum*. Monkeys were anesthetized with either Ketamine, 7-10 mg/kg, IM or Telazol, 3-5 mg/kg, IM. Blood samples were obtained by venipuncture of the femoral vein using a vacutainer and vacuum tubes. Serum was collected and stored at -80 degrees C until assayed.

Ex vivo glucose uptake

Ex vivo glucose uptake in EDL and soleus muscle was measured previously described (Bruning et al., 1998), with two main modifications: first, ^{3}H-2-deoxyglucose (^{3}H-2DG, 1.5 μCi/ml) but not ^{14}C-mannitol, was used. Second, EDL and soleus muscles were processed as follows to separate ^{3}H-2DG and ^{3}H-2DG-6-phosphate. EDL and soleus muscles were homogenized in 500 μl water and boiled for 10 min immediately after. After that, homogenates were spin at max speed for 10 min. 50 μl of the supernatant were added to 450 μl of water and counted in 5 ml of scintillation liquid. 400 μl were passed through an anion exchange column (AG 1-X8 resin, Bio-Rad) to remove ^{3}H-2DG-6-phosphate. Column was washed with 2 ml of water and 500 μl of the eluted volume were counted in 5 ml of scintillation liquid. The difference between the total and eluted ^{3}H radioactivity represents ^{3}H-2DG-6-phosphate accumulated in the tissue.

In vivo glucose uptake

For in vivo glucose uptake, a modification of a previously described method (Howlett et al., 2013) was used with some modifications. An initial pilot experiment with a group of WT resting and WT exercising mice was performed to validate the method. Briefly, mice were injected prior to exercise with 10 μCi of ^{3}H-2-deoxyglucose (^{3}H-2DG) in 100 μl of 0.9% NaCl. Next, mice were placed on a treadmill and were forced to run for 40 min at a constant speed (30cm/s). After exercise, blood glucose and quadriceps muscles were collected to determine ^{3}H radioactivity. ^{3}H radioactivity in blood was similar in all mice, indicating similar systemic delivery of the tracer. To determine ^{3}H-2DG-6-phosphate accumulation in the tissue, muscles were processed as follows: white and red quadriceps

muscles were homogenized in 1 ml of water and boiled for 10 min immediately after. After that, homogenates were spin at max speed for 10 min. 50 μl of the supernatant were added to 450 μl of water and counted in 5 ml of scintillation liquid. 900 μl were passed through an anion exchange column (AG 1-X8 resin, Bio-Rad) to remove ^{3}H-2DG-6-phosphate. Column was washed with 6 ml of water and 500 μl of the eluted volume were counted in 5 ml of scintillation liquid. The difference between the total and eluted ^{3}H radioactivity represents ^{3}H-2DG-6-phosphate accumulated in the tissue.

Transfection of C2C12 myoblasts for analyses of GLUT4 translocation

The day before transfection, C2C12 myoblasts were plated in 6-well plates (100,000 cells/well). Cells were co-transfected with HA-glut4-gfp and Gprc6a-myc plasmids using Lipofectaine 2000® (Invitrogen) at a ratio 1:4 (μg DNA:μl Lipofectamine 2000®) in combination with 2 μl of CombiMag™ (OZBiosciences) magnetic nanoparticles in Opti-MEM™ (Invitrogen) media. Cells were incubated with the mix for 30 min on a magnetic plate at room temperature. 8 h after transfection, cells were cultured in complete growth media (DMEM high glucose, 10% FBS, 1% penicillin/streptomycin). 24 h after transfection cells were used for the analyses of GLUT4 translocation as previously described (Zeigerer et al., 2002).

Energy metabolism in myofibers

For energy metabolism studies myofibers were isolated from flexor digitorum brevis muscle and used in all experiments after an overnight incubation in

matrigel-coated plates with DMEM high glucose containing penicillin/streptomycin, gentamycin, pyruvate and 2% FBS. For mitochondrial function studies, the Seahorse XF Cell Mito Stress Test Kit was used following manufacturer's protocol. To determine glucose or FAs utilization, myofibers were incubated in a non-CO_2 incubator for 4 h in KHRB containing exclusively glucose (25 mM) or oleic acid (3 mM) following by the measurement of oxygen consumption rates (OCR). To determine glycolysis, myofibers were cultured in DMEM high glucose containing penicillin/streptomycin, gentamycin, pyruvate but no FBS, for 4 hours. After that, myofibers were treated with vehicle, osteocalcin or other Gprc6a ligands for 1 hour. After treatment, myofibers were incubated with Seahorse XF Assay Medium containing 1 mM glutamine and vehicle, osteocalcin or other Gprc6a ligands for 1 hour in a non-CO_2 incubator and then ECAR was measured before and after the addition of glucose.

Metabolite Profiling

Liquid Chromatography/Mass Spectrometry (LC/MS). Plasma samples were processed using module 1, and tissue samples using module 1 and module 3, at the Einstein Stable Isotope and Metabolomics Core Facility (see http://www.einstein.yu.edu/research/shared-facilities/stable-isotope-metabolomics-core/services/).

Module 1 employs a targeted metabolomics approach using the Absolute IDQ p180 kit (BIOCRATES Life Sciences AG, Innsbruck, Austria) that has proved useful in predicting disorders in fuel homeostasis (Krug et al., 2012; Wang-Sattler et al., 2012). The kit allows simultaneous quantification of 40 acylcarnitines, 90

glycerophospholipids (lysophosphatidylcholine and phosphatidylcholine) and 15 sphingolipids by Flow Injection analysis-Mass Spectrometry (FIA-MS/MS) and 21 amino acids and 20 amino acid metabolites/biogenic amines by LC/MS. The settings follow the manufacturer's instruction for UPLC-MS/MS using the Aquity UPLC and the Xevo TQ MS (Waters, Pittsburgh, PA, USA).

Module 3 employs LC/MS/MS (Waters Xevo TQ). Analysis was used for quantitation of glycolytic, pentose and TCA cycle metabolites as per (Serasinghe et al., 2015). For glycolytic, pentose, and TCA metabolites, chromatographic analysis prior to targeted, multiple reaction monitoring (MRM) mass spectrometric analyses, was performed using an Aquity UPLC using a Waters BEH amide 1.7 µm column 2.1 x 100 mm, and an acidic mobile phase containing an acetonitrile/water gradient, as per (Serasinghe et al., 2015). Samples were bracketed in between calibration standards and linear regression was performed for quantitation.

LC/MS sample preparation. For plasma samples using module 1, 10 µl was spotted per well and processed as per kit instructions. For the skeletal muscle samples, the same extract was used for both modules 1 and 3. Approximately 50 mg of tissue was used per assays. The tissue samples were homogenized with 7 times volume of methanol (with 5mmol ammonium acetate) for the sample weight. 2 µg of internal standard ($U^{13}C$-succinate) was added to each sample prior to homogenization, after which samples frozen in liquid nitrogen were thawed on ice, sonicated and again freeze thawed. The supernatant was used for analysis.

Gas Chromatograph-Time of Flight Mass Spectrometry (GC-TOF MS) sample preparation. The samples were homogenized using10 fold volume to the weight of skeletal muscle tissue, with methanol containing (3 internal standards, 25μM of $U^{13}C$-citrate, 15μM of $U^{13}C$ succinate and 150μM of heptadecanoic acid). After addition of methanol to muscle sample, the sample was homogenized, then an equal volume water was added, homogenized again, frozen in liquid nitrogen, thawed on ice, sonicated and again freeze thawed, The supernatant was used for analysis. After lyophilization, the samples were methoximized with 50 µl of methoxyamine hydrochloride (MOA, 15 mg/mL in pyridine) at 30 ^{0}C for 90 min. The silylation step was done with 50 µl of N,O-Bis(trimethylsilyl) trifluoroacetamide (BSTFA, containing 1% TMCS) at 70 ^{0}C for 60 min, as per (Qiu et al., 2014).

GC-TOF MS Analysis. The samples were analyzed using a Water GC-TOFMS Premier (Waters, USA) in electron impact ionization (EI) mode. The samples were injected at 270^{0}C with a split ratio of 10. Metabolites separation was performed on a 30-meter DB-5MS column coupled with 10-meter guard column (Agilent, USA). The initial oven temperature was set to 60 ^{0}C and kept for 1 min, then rise to 320 ^{0}C at a rate of 10 ^{0}C/min and kept for 3 min. Helium was used as carrier gas at a consistent flow rate of 1ml/min. The transfer line and the source temperature were set at 250 ^{0}C and 220^{0}C, separately.

Data Analysis. A pooled quality control (QC) sample, comprised of equal amounts from all samples, was injected every 10 samples, regardless of MS method, and the multiple QC injections were used to calculate the coefficient of

variation (CV = standard deviation/mean) for each metabolite. Metabolites having CVs greater than 30% were not considered accurate enough for consideration, and also 75% of all measured sample concentrations for the metabolite should be above the limit of detection (LOD). To select candidate biomarkers, principal component analysis (PCA) and Partial Least Squares Discriminant Analysis (PLS-DA) were used.

^{13}C-glucose tracer studies

The contribution of glucose oxidative metabolism was assessed using mass spectrometry and ^{13}C stable isotope tracer technology. The fractional contributions to the CAC, amino acids and lactate were assayed in muscle homogenates using methods as previously described (Kombu et al., 2011; Zhang et al., 2015). This approach enables isotopically labeled metabolites to be measured with a high degree of sensitivity, following a bolus of $^{13}C_6$ glucose tracer.

GC-MS assays. Following homogenization and centrifugation, the supernatant fractions were decanted and reserved for measurements of concentrations and [^{13}C]label of acetyl-CoA enrichment. The tissue pellets were further extracted using a mixture of acetonitrile and 2-propanol (3:1), centrifuged and then analyzed for CAC, amino acids and related intermediates. Extracts were then dried by nitrogen gas for 1-2 hours and chemically derivatized using MTBSTFA + 1% TBDMCS reagent (N-methyl-N-(tert-butyldimethylsilyl) trifluoroacetamide + 1% tert-butyldimetheylchlorosilane, Regis Technologies, Inc. Morton Grove, IL, USA) at reacted at 70 °C for 30 min. The derivatized products were measured

under Agilent 6890 Gas-Chromatography and Agilent 5973 Mass Spectrometry (GC-MS). A DB-17 MS capillary column (30m × 0.25mm × 0.25 μm) was used in all analysis. The starting oven temperature was set to 80 °C, the pressure was 14.82 psi, and the flow velocity was 45cm/sec. Temperature was then increased to linearly to 220 °C and held for 1 min. The mass spectrometer was in electron-impact (EI), sim mode. CAC and related intermediates, succinate (m/z= 289), fumarate (m/z =287), malate (m/z =419), citrate (m/z=459) were measured. Other intermediates and amino acids, including 3-hydroxyglutarate (m/z= 433), aspartate (m/z =418), glutamate (m/z =432), glutamine (m/z =431) and GABA (m/z =274) were also measured.

The plasma glucose enrichment was measured using a GC-MS method. Briefly, the plasma glucoses were dried and incubated with 100 μl of pyridine:acetic anhydride (2:3) at 75 °C for 30 min. An Agilent 6890 GC system were used to determine the selective ion (Ammonia chemical ionization; CI) m/z 408-414.

*LC-MS assays***.** Acetyl-CoA and succinyl-CoA in muscle was measured by LC-MS methods. Briefly, the supernatant fraction was loaded onto a Supelco solid-phase extraction cartridge ([2-(pyridyl)-ethyl functionalized silica gel] preconditioned with 3 ml of methanol and then added 3 ml of buffer A (1:1 methanol-H_2O with 2% acetic acid). The cartridge was then washed with 3 ml of buffer A to elute impurities, followed sequentially by 3 ml of buffer B (1:1 methanol-H_2O with 50 mM ammonium formate), 3 ml of buffer C (3:1 methanol-H_2O with 50 mM ammonium formate), and 3 ml of methanol to elute the acyl-CoAs. The eluent was evaporated under nitrogen.

The LC was coupled with an API4000 Qtrap Mass Spectormeter (Applied Biosystems, Foster City, CA) operated under positive ionization. Acetyl-CoA was m easured at the 14.2 min elution time and the ions 810/303 – 812/305 were monitored.

Calculations

Fractional contributions of [$^{13}C_6$]glucose to oxidaitve metabolism.The fractional isotopic enrichments (via ^{13}C label incorporation) for each of the intermediates were defined as molar percent enrichment (MPE), after background correction. The MPEs (unit: percent) is calculated as

$$MPE_{(M+n)} = 100 \times \frac{A_i}{\sum_{i=0}^{n} A_i}$$

Where $MPE_{(M+n)}$ is the *n* th ^{13}C labeled mass isotopomer enrichment of the metabolite. *A* is the abundance (arbitrary unit) measured by GC-MS. The variable *i* varied from zero to *n*, while *n* is no more than 6. $A_{(0)}$ is the abundance non-labeled metabolite, and $A_{(i)}$ is the abundance for mass isotopomer labeled with i ^{13}C, regardless of position.

The M+2 (M2) MPE of each of the intermediates reflected the contribution of [$^{13}C_6$]glucose to that intermediate pool. For the measurements of the contribution of [$^{13}C_6$]glucose to oxidative metabolism, the assumption was that the first turn of the CAC produces mostly M+2 [^{13}C]labeled intermediates from [1,2-^{13}C]acetyl-CoA via pyruvate dehydrogenase complex (PDH). Thus, the first turn of the CAC (as measured by M+2 for each intermediates) reflected oxidative metabolism.

Concentrations of intermediates in tissue. The concentrations of the endogenous tissue metabolites were determined by standard curves for each metabolite and the known amount internal standard added to the sample. For the absolute concentrations of fumarate, malate and succinate, internal standards of [$^{13}C_4$] succinate, or (*RS*)-3-hydroxy-[$^{2}H_4$]glutarate were used; glutamine and glutamate concentrations were calculated using [$^{2}H_5$]glutamate or [$^{2}H_5$] glutamine; the acetyl-CoA and succinyl-CoA concentrations were assayed using an internal standard of [$^{2}H_9$]pentanoyl-CoA.

Muscle contractility

Contractile measurements were performed on fast twitch muscle EDL and slow twitch muscle Soleus. Both muscles were dissected from hind limbs and placed in chilled Krebs solution (in mM: 119 NaCl, 4.7 KCl, 2.5 CaCl2, 1.2 KH2PO4, 1.2 MgSO4, 20 NaHCO3, bubbled with 95% O2-5% CO2 (pH 7.4). The tendons of the muscles were tied to a force transducer (400A, Aurora Scientific) and an adjustable hook using nylon sutures. The muscles were immersed in a stimulation chamber containing the Krebs solution continuously bubbled (O_2 95/ Co_2 5%) (at 28°C). The muscle was stimulated to contract using an electrical field between two platinum electrodes (Aurora Scientific 1200A - in vitro System).

The muscle length (Lo) was first adjusted to yield the maximum force. The force–frequency relationships were determined by triggering contraction using incremental stimulation frequencies (0.5 ms pulses at 10–120 Hz for 350 ms at supra- threshold current). Between stimulations the muscle was allowed to rest for ~1 min. Fatigability of the muscles was assessed by measuring the loss of

force in response to repeated stimuli (30 Hz, 300 ms duration) at 1Hz over 10 min. After the measurements of contractile properties were completed, muscles were measured at Lo, dried to remove the buffer, and weighed. The muscle cross-sectional area was determined by dividing muscle weight by its length and tissue density (1.056 g/cm3). Force production was then normalized to the muscle cross-sectional area to determine the specific force.

Muscle Histomorphometry

For mitochondria histomorphometry, EDL and soleus muscles were fixed in 4% PFA/2% glutaraldehyde/0.1M sodium cacodylate pH 7.3, post-fixed in 1% osmium tetraoxide and embedded in epoxy resin (Epon). Ultrathin sections (80 nm) were stained with aqueous uranyl acetate and lead citrate and examined with a JEOL 2000FX transmission electron microscope. For the determination of the cross-section area of muscle fibers, gastrocnemius muscle was fixed in 10% neutral formalin, embedded in paraffin and sectioned at 5μm. Sections were stained with hematoxylin and eosin and analyzed using the ImageJ software. For determination of muscle fiber type composition, gastrocnemius muscle was frozen in liquid N_2-cooled methylbutane. Samples were sectioned at 10μm. SDH, ATPase and COX activity assays were performed as described (Quiat et al., 2011). Images were analyzed using the ImageJ software.

RNASeq

RNA was extracted from each group using RNAqueous®-Micro Total RNA Isolation Kit (ThermoSci, #AM1931) and the quality of purified RNA samples was determined using a Bioanalyzer 2100 (Agilent) with an RNA Pico kit. Extracted

RNA samples were amplified by Ovation® RNA-Seq System V2 (NuGEN) Kit. Amplified cDNA was labeled with Encore biotin module Kit (NuGEN) for RNASeq applications Illumina Truseq RNA Sample Prep v2 using the LT protocol. RNA was sequenced at 30M paired 100 bp reads reads per sample on an Illumina 2500 HISeq instrument.

Bases were called with Illumina's Real Time Analysis (RTA 1.9) (Illumina, 2015b). Adaptors were trimmed and reads were converted from BCL to Fasta format with bcl2fastq 1.8.4 (Illumina, 2015a). Reads were mapped to the mm9 mouse genome with Bowtie2 (Langmead and Salzberg, 2012) 2.0.0-beta7 and TopHat2 (Kim et al., 2013) 2.0.4. Reads were counted with HTSeq-0.6.1p2 (Anders et al., 2015). These data were deposited in the Gene Expression Omnibus (GEO) (Barrett et al., 2013), Accession number, GSE75919.

Experiments were normalized with TMM (Robinson and Oshlack, 2010). Differential expression was estimated using Limma-Voom with weights (Law et al., 2014; Liu et al., 2015). All of the Benjamini-Hochberg (Benjamini and Hochberg, 1995) False discovery rates (fdr) were > 0.90. However, spot checking key genes by PCR, shows that an uncorrected $p \leq 0.02$ is a reliable significance cutoff for this RNASeq experiment. 242 genes were statistically significantly differentially expressed by this cutoff.

To visualize the effect of osteocalcin signaling in myofibers on gene expression independently of the magnitude of expression of each gene, raw counts for a gene were divided by the total number of counts for that gene across samples, and then $\log_2$ transformed. In addition, clustering of all genes which were

differentially expressed with p≤0.02 and range(log_2(normalized-counts)) ≥ 1 (46 genes) was performed (Figure 5A). Clustering was performed with Cluster 3.0 (de Hoon et al., 2004; Eisen et al., 1998). The expression of each gene, and then samples, were mean centered. Both genes and samples were clustered using average-linkage clustering (Everitt et al., 2011). The heatmaps were displayed with JavaTreeView (Saldanha, 2004).

Statistics

All data are presented as mean ± standard error of mean. Statistical analyses were performed using unpaired, two-tailed Student's t test for comparison between two groups and ANOVA test for experiments involving more than two groups. For all experiments, * denotes P ≤ 0.05, ** P ≤ 0.005.

Supplemental References

Anders, S., Pyl, P.T., and Huber, W. (2015). HTSeq--a Python framework to work with high-throughput sequencing data. Bioinformatics *31*, 166-169.

Barrett, T., Wilhite, S.E., Ledoux, P., Evangelista, C., Kim, I.F., Tomashevsky, M., Marshall, K.A., Phillippy, K.H., Sherman, P.M., Holko, M.*, et al.* (2013). NCBI GEO: archive for functional genomics data sets--update. Nucleic Acids Res *41*, D991-995.

Benjamini, Y., and Hochberg, Y. (1995). Controlling the false discovery rate; A practical and powerful approach to multiple testing. J Roy Stat Soc Ser B *57*, 289-300.

Bruning, J.C., Michael, M.D., Winnay, J.N., Hayashi, T., Horsch, D., Accili, D., Goodyear, L.J., and Kahn, C.R. (1998). A muscle-specific insulin receptor knockout exhibits features of the metabolic syndrome of NIDDM without altering glucose tolerance. Mol Cell *2*, 559-569.

de Hoon, M.J., Imoto, S., Nolan, J., and Miyano, S. (2004). Open source clustering software. Bioinformatics *20*, 1453-1454.

Eisen, M.B., Spellman, P.T., Brown, P.O., and Botstein, D. (1998). Cluster analysis and display of genome-wide expression patterns. Proc Natl Acad Sci USA *95*, 14863-14868.

Everitt, B.S., Landau, S., and Leese, M. (2011). Cluster Analysis (Wiley).

Howlett, K.F., Andrikopoulos, S., Proietto, J., and Hargreaves, M. (2013). Exercise-induced muscle glucose uptake in mice with graded, muscle-specific GLUT-4 deletion. Physiol Rep *1*, e00065.

Illumina (2015a). bcl2fastq Conversion Software (Illumina).

Illumina (2015b). Real Time Analysis (RTA).

Kim, D., Pertea, G., Trapnell, C., Pimentel, H., Kelley, R., and Salzberg, S.L. (2013). TopHat2: accurate alignment of transcriptomes in the presence of insertions, deletions and gene fusions. Genome Biol *14*, R36.

Kombu, R.S., Brunengraber, H., and Puchowicz, M.A. (2011). Analysis of the citric acid cycle intermediates using gas chromatography-mass spectrometry. Methods Mol Biol *708*, 147-157.

Krug, S., Kastenmuller, G., Stuckler, F., Rist, M.J., Skurk, T., Sailer, M., Raffler, J., Romisch-Margl, W., Adamski, J., Prehn, C.*, et al.* (2012). The dynamic range of the human metabolome revealed by challenges. FASEB J *26*, 2607-2619.

Langmead, B., and Salzberg, S.L. (2012). Fast gapped-read alignment with Bowtie 2. Nat Methods *9*, 357-359.

Law, C.W., Chen, Y., Shi, W., and Smyth, G.K. (2014). voom: Precision weights unlock linear model analysis tools for RNA-seq read counts. Genome Biol *15*, R29.

Liu, R., Holik, A.Z., Su, S., Jansz, N., Chen, K., Leong, H.S., Blewitt, M.E., Asselin-Labat, M.L., Smyth, G.K., and Ritchie, M.E. (2015). Why weight? Modelling sample and observational level variability improves power in RNA-seq analyses. Nucleic Acids Res *43*, e97.

Qiu, Y., Cai, G., Zhou, B., Li, D., Zhao, A., Xie, G., Li, H., Cai, S., Xie, D., Huang, C.*, et al.* (2014). A distinct metabolic signature of human colorectal cancer with prognostic potential. Clin Cancer Res *20*, 2136-2146.

Quiat, D., Voelker, K.A., Pei, J., Grishin, N.V., Grange, R.W., Bassel-Duby, R., and Olson, E.N. (2011). Concerted regulation of myofiber-specific gene expression and muscle performance by the transcriptional repressor Sox6. Proc Natl Acad Sci U S A *108*, 10196-10201.
Robinson, M.D., and Oshlack, A. (2010). A scaling normalization method for differential expression analysis of RNA-seq data. Genome Biol *11*, R25.
Saldanha, A.J. (2004). Java Treeview--extensible visualization of microarray data. Bioinformatics *20*, 3246-3248.
Serasinghe, M.N., Wieder, S.Y., Renault, T.T., Elkholi, R., Asciolla, J.J., Yao, J.L., Jabado, O., Hoehn, K., Kageyama, Y., Sesaki, H.*, et al.* (2015). Mitochondrial Division Is Requisite to RAS-Induced Transformation and Targeted by Oncogenic MAPK Pathway Inhibitors. Mol Cell *57*, 521-536.
Wang-Sattler, R., Yu, Z., Herder, C., Messias, A.C., Floegel, A., He, Y., Heim, K., Campillos, M., Holzapfel, C., Thorand, B.*, et al.* (2012). Novel biomarkers for pre-diabetes identified by metabolomics. Mol Syst Biol *8*, 615.
Zeigerer, A., Lampson, M.A., Karylowski, O., Sabatini, D.D., Adesnik, M., Ren, M., and McGraw, T.E. (2002). GLUT4 retention in adipocytes requires two intracellular insulin-regulated transport steps. Mol Biol Cell *13*, 2421-2435.
Zhang, Y., Zhang, S., Marin-Valencia, I., and Puchowicz, M.A. (2015). Decreased carbon shunting from glucose toward oxidative metabolism in diet-induced ketotic rat brain. J Neurochem *132*, 301-312.